TAMPEREEN TEKNILLINEN YLIOPISTO
TAMPERE UNIVERSITY OF TECHNOLOGY

SYED AHSAN ABBAS

OPTICAL PROJECTION TOMOGRAPHY AS A TOOL TO ANALYZE 3D CELL CULTURES OF CARDIOMYOCYTES

Master of Science thesis

Examiner: Prof. Jari Hyttinen
Examiner and topic approved by the Faculty of Natural Sciences on 9th September 2015

ABSTRACT

SYED AHSAN ABBAS: Optical Projection Tomography as a tool to analyze 3D cell cultures of cardiomyocytes
Tampere University of technology
Master of Science Thesis, 47 pages, 11 Appendix pages
June 2014
Master's Degree Programme in Science and Bio engineering
Major: Bioimaging
Examiner: Professor Jari Hyttinen

Keywords: cardiomyocytes, hydrogel, imaging, optical projection tomography, acquisitions, motion analysis, traction force

This Master's thesis addresses the issue of the possibility of the imaging and analysis of the live cardiomyocytes' clusters using Optical projection tomography. Cardiomyocytes are heart muscle cells that play an important role in the beating of the heart. Research scientists have been imaging beating cardiomyocytes using traditional phase contrast microscopy techniques. The Optical projection tomography technique involves placing a biological sample in the refractive index matching bath, for instance distilled water for gel-based samples because of the matching refractive index value, after which the sample is illuminated with the bright field light and the images are acquired using either a LabView or an HCImageLive program.
Since, the Optical projection tomography is relatively a new technology and it is deemed more optimized for larger and static samples such as tissues and embryos etc. therefore, it is quite challenging to prove the efficacy of the Optical projection tomography method for imaging smaller and faster aggregates of cardiomyocytes. At first, cardiomyocytes are differentiated and produced from the human induced pluripotent stem cells at Heart Group, BioMediTech, UTA. After differentiation, live cardiomyocytes are placed in 3D hydrogel and imaged using Optical projection tomography. The samples are imaged using customized LabView program and HCImageLive program. The imaging method deploys an acquisition of 400-1000 images of the samples on different focal planes. In this regard, samples are rotated at different focal angles to visualize the beating pattern at different angular positions. After the continuous acquisitions are obtained, the videos of the live cardiomyocytes are constructed from the continuous frames of images using ImageJ. Once, the videos of the beating cardiomyocyes are constructed, both qualitative and quantitative analyses are done on the beating aggregates using analysis tools on MATLAB and ImageJ plugins, PIV (Particle Image Velocimetry) and FTTC (Traction force microscopy). The analysis focuses on the traction forces of the live cardiomyocytes.
Results show that the Optical projection tomography technique can be successfully used for the imaging and characterization of the beating clusters of cardiomyocytes. Furthermore, the images and videos obtained from the Optical projection tomography technique are good for analysis using different software tools.

PREFACE

This thesis was done in collaboration with the Department of Electronics and Communication Engineering, Tampere University of Technology and BioMediTech, FinnMedi.

First and foremost, I cannot thank Allah Al-Mighty enough for making me succeed in my goals and acquire funded position at BioMediTech. Likewise, Salutations and Peace be upon Prophet Muhammad and His Progeny.

I would like to state that working at BioMediTech has been such a wonderful experience especially I might never ever get a Boss kinder and sweeter than Professor Jari Hyttinen. I am highly grateful to him for his continuous support in terms of believing in me, being very kind and easy-going and also for choosing me for the funded position. Moreover, he has never put any kind of unnecessary pressure on me. I thank him again for not only being a wonderful supervisor but also, an amazing human being. Similarly, I would like to extend my sincere gratitude to the co-supervisor Edite Figueiras without whom I would never ever be able to learn much about OPT. It is because of her that I learned everything about using OPT right from the acquisitions to the video construction etc. Both Jari and Edite are the epitome of all the attributes of an ideal mentor. I cannot thank both of them enough for especially reviewing my Master's thesis plenty of times and pointing out the needed amendments. It is because of their valuable suggestions that my Master's thesis looks presentable now.

I am also highly grateful to Janne Koivisto who has always helped with the culturing and preparation of the cells. He has been very kind and always willing to provide us with the samples no matter what. I owe him even more now at the end of my thesis writing process since he also took out his valuable time to go through my thesis and added his valuable suggestions and comments, especially about the cell culturing part.

I am also thankful to Antti Ahola since he was the one who helped me with the motion analysis using MATLAB. I would also like to thank Marie, Toni, Olli and Heidi for being very nice colleagues. I will always remember all the funny conversations I would have with Toni in the OPT room.

Last but not the least, I would like to not only thank but also dedicate my Master's thesis to my Parents and my brother. They have always had a great confidence in me. I owe them a great deal of gratitude for without them, I would never have gone this far.

Syed Ahsan Abbas

Tampere, 25.11.2015

CONTENTS

LIST OF FIGURES

LIST OF SYMBOLS AND ABBREVIATIONS

AFM	Atomic force microscopy
ATP	Adenosine triphosphate
ECM	Extracellular matrix
END 2	Endodermal-like cells
FEP	Fluorinated Ethylene Propylene
FFT	Fast Fourier Transform
FTTC	Fourier transform traction cytometry
hESCs	Human embryonic stem cells
HMT 3522	Cancerous cells
In vitro	in an artificial environment outside the living organism
In vivo	within a living organism
iPS	(Human) induced pluripotent stem (cells)
LabView	Laboratory visual instrument engineering workbench
LSCM	Laser scanning confocal microscopy
Obj. L	Objective lens
OPT	Optical Projection Tomography
PIV	Particle Image Velocimetry
RyRs	Ryanodine receptors
SEM	Scanning electron microscope
TUT	Tampere University of technology
UTA	University of Tampere
WFDI	Wide-field digital interferometry
X-Ray µCT	X-ray micro computed tomography
2-D	Two dimensional
3-D	Three dimensional

A	Bright-field illumination module
B	Detection module
L1	white LED
L2	Telecentric backlight illuminator
L3	Tube lens
P	Pinhole

1. INTRODUCTION

Cardiomyocytes, as their name suggests, are heart muscle cells that form the heart muscle. These cardiac muscle cells, along with the pacemaker cells, play a vital role in the beating of the heart. Like pacemaker cells, cardiomyocytes have also been a prime research focus of the researchers studying the development and disease modelling of the heart. The very first stage to do the research on cardiomyocytes requires researchers to acquire live cardiomyocytes through different cell culturing methods. In this regard, scientific articles discuss different possibilities of obtaining cardiomyocytes through cells differentiation methods. A scientific study, published in year 2005, documented the differentiation of the adult murine skeletal muscle cells into beating cardiomyocytes with the use of video microscopy and electron microscopy techniques. [1].

Another relatively recent research study conducted in year 2014, focused on the use of non-invasive digital image correlation method to analyze the single beating cardiomyocytes [2] but our research study takes into account the analysis of the beating aggregates instead of the single beating cells. Another limitation with some of the existing research studies and techniques is their limitation to 2-D [2, 3] while the use of a 3-D technique such as laser scanning confocal microscopy [4] has also been found to have an oversampling problem [5]. There is also a lack of availability of the pre-existing images and videos of the beating of the aggregates of cardiomyocytes in 3-D. Moreover, the existing work in this regard comprises of using traditional phase contrast microscopy techniques. On the other hand, Optical projection tomography (OPT) is a very effective three-dimensional (3-D) imaging technique that is successfully used to image small biological samples [6]. However, the use of OPT technique to image the beating clusters of cardiomyocytes has not been reported previously. In an OPT setup; a biological sample is placed in a sample holder which is rotated at certain angular increment (usually 0.9 degree) and an image is taken at each angular step. Hence, an OPT technique can be used to do the acquisitions over complete 360 degree rotations of the sample.

The objective of this thesis is very novel and unique as there is no existing published data available on any kind of exactly similar work. The goal of the thesis work is to do the imaging experiments and analysis of the 3-D cultures of the beating aggregates of cardiomyocytes with the use of Optical projection tomography (OPT) technique.

The cardiomyocytes, used in the research work, were differentiated from the human induced pluripotent stem (iPS) cells. It must be especially noted that the stem cells have the self-renewal capability and they can also differentiate into other cells with special-

ized functions [7]. In addition, the use of stem cells to produce cardiomyocytes is not deemed unethical and adult stem cells can be easily isolated as well [8].

Following the image acquisitions of the beating aggregates of cardiomyocytes, we performed the motion analysis of the acquisitions using MATLAB motion analysis tool [2]. Also, an approximate evaluation of the average traction forces was carried out using ImageJ software. Briefly, an experiment was setup to calculate the average traction force values of the sample at three different temperature values.

We took into account both qualitative and quantitative analytical methods in order to evaluate the efficacy of OPT technique for the imaging and analysis of 3-D cell cultures of cardiomyocytes.

2. THEORETICAL BACKGROUND

Optical Projection Tomography is a non-invasive, and hence non-destructive, three dimensional imaging technique which can be successfully used to image small samples that are in the mesoscopic range [8, 9]. This technique is often seen as having similarities with the X-ray computed tomography except for the difference of the use of the parallel ray projection in OPT whereas X-ray computed tomography utilizes fan beam projection technique.

Since, our research work comprises of the imaging and analysis of the beating clusters of cardiomyocytes therefore, this chapter discusses all the theoretical aspects of the research topic right from the production of cardiomyocytes to the analysis of the cell movements.

2.1 Cardiomyocytes

Cardiomyocytes, along with pacemaker cells, play an important role in the beating of the heart. The cardiac pacemaker cells are responsible to generate and carry out electrical impulses that are responsible for the beating of the heart. They also transmit electrical impulses from one cell to another. On the other hand, cardiomyocytes are the ones that form the cardiac muscle. Also referred to as cardiac myocytes, they are responsible for pumping over 7000 litres of blood per day [10].

Cardiomyocytes contain myofibrils, which are composed of proteins and sarcomeres and bring about the coordinated contractions of the cardiomyocytes. The onset of action potential and excitation waves across the plasma membranes of adjacent cardiac cells causes the release of the calcium from the sarcoplasmic reticulum which, in turn, results in the contraction of myofibrils [10]. This helps in pumping and propelling the blood out of the chambers to the circulatory systems. The cardiomyocytes also heavily produce adenosine triphosphate (ATP) very quickly which makes them extremely resistant to fatigue.

In addition, cardiomyocytes are electrically and mechanically connected with each other through the intercalated disks [10]. This keeps the cardiomyocytes integrated and also brings about coordinated contractions of the heart muscle.

2.1.1 Importance of human stem cell-derived cardiomyocytes

In the recent years, due to the rising demand for drug development and toxicity testing, studies based on stem cell-derived cardiomyocytes have gained a lot of importance and attention. Cardiotoxicity is one of the major problems associated with cardiovascular research. It hinders the drug development process. The use of traditional in vitro (in an artificial environment outside the living organism) non-cardiac cell models and animal models lack the ideal mimicking of in vivo (within a living organism) cardiomyocytes [11] and hence there is a greater need of drug screening and toxicity studies based on human stem cell-derived cardiomyocytes.

In this regard, potential benefits of induced pluripotent stem cell-derived cardiomyocytes have been studied for drug development and toxicity studies [11, 12]. Daniel *et al.* (2014) [12] have published a summary of the disease modeling studies in which patient-specific induced pluripotent stem cells were used for heart disease modeling.

In another study, Caspi O *et al.* (2009) [13] have highlighted the possibility of the utilization of human embryonic stem cell-derived cardiomyocytes for in vitro electrophysiological drug testing and for the study of cardiac arrhythmias.

Thus, human stem cell-derived cardiomyocytes play a crucial and instrumental role in heart disease modeling, toxicity studies and drug screening [11-13].

2.1.2 Production of cardiomyocytes using stem cells

Cardiomyocytes can be produced by stem cells though differentiation methods. For instance, Pluripotent stem cells, human embryonic stem cells (hESCs) and human induced pluripotent stem (iPS) cells can be differentiated into live cardiomyocytes using different methods [14-17]. Moreover, stem cells are the cells characterized by two distinguished characteristics, self-renewal and differentiation. Stem cells are capable of renewing themselves through cell division, while they can also be differentiated to form tissue-specific cells with special functions [7]

Even though our research study focuses on the production of human cardiomyocytes but the use of primary rat cardiomyocytes has also been reported previously in other research studies [18-20]. The reason why primary rat cardiomyocytes are found to be generally used for the in vitro research work is the ease with which they can be easily isolated in large numbers with a single procedure.

It must be especially noted that Louch WE *et al.* (2011) [19] described several different methods to isolate and culture adult and neonatal ventricular myocytes from rat and mouse heart. The article carries an appropriate and detailed description of the various methods that are used for both isolation and culture of adult and neonatal myocytes [19]. In addition, Roth GM *et al.* (2014) [20] have presented a descriptive protocol of

isolating rat cardiomyocytes using Langendorff perfusion. It has also been argued that isolation of cardiomyocytes via perfusion is also the best method to study and keep a track of the cellular changes that might lead to heart failure under some experimental conditions [20].

As far as human cardiomyocytes are concerned, they are derived from the stem cells. The human heart itself is not highly capable to regenerate and repair, for instance, following myocardial infarction. However, the development and advancement in the stem cell technology has brought about the new ideas and methods that can be implemented to help treat cardiac disorders. There are numerous differentiation methods with which pluripotent stem cells, human embryonic stem cells (hESC) and induced pluripotent stem (iPS) cells can be made to differentiate into functional cardiomyocytes [14-17]. In addition, scientists also argue that the adult stem cells that are highly capable of differentiating into beating cardiomyocytes are cardiac progenitor cells [21- 22]. Besides, quite many other research studies also talk about differentiation of human embryonic stem cells into beating cardiomyocytes [22-24]

2.2 Hydrogels

Hydrogels are water-swollen polymeric networks that maintain their solid form due to the presence of cross-links. Moreover, hydrogels are three dimensional and are composed of hydrophilic polymers. There has been a drastic increase in the use of natural polymer based hydrogels in the field of biomedical sciences, tissue engineering and particularly, for regenerative medicine purposes. This prodigious rise and demand in the use of hydrogels come from their excellent and promising mechanical and physiochemical properties.

Hydrogels are highly biocompatible, can be mechanically strong and on top of all, easy to prepare. Hydrogels, in regenerative medicine, are used as scaffolds that serve as medium providers for cells where they adhere, proliferate, differentiate and develop into tissue. They can also provide mechanical and chemical signals which result in enhanced reparative processes and morphogenic guidance. Hydrogel based regenerative medicines have been found to be beneficial and useful for tissues such as cartilages, bones, muscles and even neurons etc.

Due to the excellent biocompatibility, hydrogels serve as the provider of the ideal three dimensional environment for the culturing of cardiomyocytes. Kathy Yuan Ye *et al.* (2011) [25] published their research work about the isolation of neonatal cardiomyocytes from three day old rat pups, subsequently followed by the preparation of the cells for encapsulation in fibrin hydrogel constructs [25].

There are various methods to prepare different types of hydrogels. Gellan gum is quite novel hydrogel in the biomedical research. Gellan gum hydrogels have adjustable me-

chanical properties. Gellan gum is a linear anionic polysaccharide composed of tetrasaccharide (1,3-β-D-glucose, 1,4-β-glucuronid acid, 1,4-β-D-glucose, 1,4-α-L-rhamnose) repeating units. Moreover, FDA has approved it as a food additive [26] which also shows how safe and biocompatible gellan gum hydrogels actually are. This fact is further strengthened by the other research studies that have shown the viability of using gellan gum hydrogels. For instance, for neural regeneration, in vivo studies on rat have shown that gellan gum hydrogels did not induce any inflammatory response upon integration into spinal cord [27].

Gellan gum hydrogels are easy to prepare. For our research work, they were conveniently prepared by combining the right amount of gellan gum (heated at 37 degree centigrade) with the bioamine cross linker (Spermine or Spermidine) in a test tube. Usually, Spermine is used as a cross linker. Furthermore, the heating of gellan gum at body temperature also ensures the biocompatibility of the gel. The preparation of gellan gum hydrogels requires preliminary preparation of stock solutions which has been explained in ***Appendix A.***

2.3 Cell culturing techniques

Cell culturing method is simply defined as the process of growing cells under the controlled conditions which is generally done outside of their natural environment [26, 27]. For instance, culture of beating cardiomyocytes is done with the heart cells cultured outside of the heart and body [18-20]. In recent years, cell culturing has become one of the most crucial and important prerequisites of the biological research.

There are two main types of cell culturing methods which are termed as two dimensional cell culturing and three dimensional cell culturing methods. We conducted our research work on three dimensional culture models of cardiomyocytes. The benefits of using 3-D cultures over 2-D cultures will be highlighted later in this chapter.

The history of cell culturing dates back to the early 19^{th} century as it was in 1907 that an American biologist and anatomist named Harrison, who was working on investigating the origin of nerve fibers, developed the method of cell culturing [28]. Harrison cultured frog neuroblasts in a lymph medium with great success which laid the foundations not only of the tissue culturing methods but also contributed to the understanding of the modern day surgical tissue transplant techniques.

The technique used by Harrison made it easier for the future scientists and biologists to understand the basics of cell and tissue culturing. He took out the pre-differentiated neural tissue from the frog embryos and placed it in a drop of lymph and kept it in sealed and in a moist chamber. Afterwards, he kept observing the tissue growth and differentiation over the course of time. [29]

2.3.1 Two dimensional (2-D) cell culturing

The technique developed by Harrison was a two dimensional cell culturing method [28]. However, there has been a considerable and drastic improvement in the 2-D cell culturing method, since it was first developed. Previously, blood plasma was usually used to provide nutrition for the growing cells but the use of blood plasma had its problems as well which included a possible allergic reaction due to antigens and a lower feasibility as compared to the use of a modern-day synthetic medium [29]. Therefore, the previous methods could not be deemed very ideal for the culturing of the beating cardiomyocytes. Nowadays, a use of synthetic medium has replaced the traditional use of the blood plasma. The batches of synthetic medium are very cost-effective and also don't carry the risk of potential allergic reactions since they do not contain antigens. There is also quite less batch-to-batch variation in a synthetic medium. Besides, other modern advancements and betterment in cell culturing practices include the use of spacious and easy-to-use cell culturing containers which result in the overall better environment for cell culture and growth, alongside ensuring the infection- free cells with the use of additives such as antibiotics and anti-fungal agents [30].

In two-dimensional cell culturing method, cells are typically grown as a monolayer, usually at a body temperature of 37 degree centigrade, on a flat surface. Flasks or petri dishes serve as the culturing containers while medium (usually synthetic) serves as a source for providing nutrition for the cells growth. However, a use of multiwell plate containing many petri dishes together is also popular.

2.3.2 Three dimensional (3-D) cell culturing

Scientists and biologists have always argued over the relevance between the 2-D cell culturing methods and in-vivo cells. Biologists argue that 2-D cell culture models may not accurately represent and relate with the in-vivo cells. This argument gave rise to developing the three-dimensional cell culturing methods which are more closely related to the in-vivo cells. In a 3-D cell culture environment, cells are allowed to grow and interact in all three dimensions across their surroundings. Also, in quite a recent scientific study, it was also found that 3-D cultures of cardiomyocytes tend to have prolonged contraction behavior as compared to 2-D cell cultures [31].

The history of three-dimensional cell culturing methods dates back to early 80's and is credited to an Iranian-American biologist Mina Bissell who highlighted the importance of using artificial 3-D extracellular matrices for producing promising in-vitro cultures of high physiological relevance. The three-dimensional cell culturing models subsequently turned out to play a key role in drug discovery applications.

In addition, three dimensional culture models have also shown better gene expression as compared to 2-D cell cultures. There are number of scientific studies that document how

a cell's microenvironment can affect the behavior of the cells in general. This fact is very well evident in a study of human breast cancer model by Weaver *et al.* (1997) [32] in which malignant cancerous cells (HMT 3522) and non-malignant HMT 3522 type breast cells were grown in 3-D using Matrigel. The normal cells were found to have formed organized acini similar to those of healthy breast tissue. On the contrary, cancerous cells resulted in the formation of unorganized aggregates. Both the malignant and non-malignant cells were treated with inhibitory beta1-integrin antibody. The results showed that the normal cells underwent apoptosis while the cancerous cells had their phenotype reversal as they appeared to become no different than normal cells, by losing their abnormal growth patterns [32]. The same results were not observed with 2-D cell cultures. In a nutshell, this study highlighted the important of 3-D extracellular matrices and their effects on the cells.

In another study related to 3-D cardiac cell culture, both 2-D and 3-D cell cultures grown from isolated primary neonatal rat cardiac ventricle cells were compared in terms of alterations in multi-cellular structures, phenotypic differences and response to hormonal stimulation [33]. This study indicated the significant alterations in both cell function and organization with the growth of cardiac ventricular cells in 3-D. Moreover, differences in tissue maturation, response to hormonal stimulation and differences in gene expression were also reported [33]. Thus, 3-D cell cultures appeared to be more helpful for the possible functional design of cardiac tissue.

Based on the above discussion, the main benefits and differences of 3-D cell culture models over 2-D cultures are briefly outlined in the Table 1.

Table 1. *2-D cell cultures versus 3-D cell cultures*

#	2-D cell cultures	3-D cell cultures
1.	Inadequate representation of living tissue's environment	Better representation of in vivo environment
2.	Limited cellular activities	Improved 3-D migration, differentiation and growth
3.	May not represent accurate gene expression	Gene expression closer to in-vivo as compared to 2-D cultures
4.	May not have longer life span as 3-D cultures	Tend to have a longer life span and hence, are also suitable for testing chronic exposure toxicity [34]

2.4 Optical Projection Tomography

Optical Projection Tomography is an imaging technique that can produce 3D images of biological specimens of up to 15 mm in size and that also, in a high resolution. The OPT technique can be successfully used for both fluorescent and non-fluorescent biological specimens [6].

The OPT technique is somewhat similar to X-ray µCT technique as in both the techniques, biological specimen is rotated at angular increments and an image is taken at each angular step. However, the evident difference between the two techniques is that OPT technique uses the light source whereas X-ray µCT utilizes an X-ray beam. Moreover, a detailed description about the OPT setup and working has been provided in Chapter 3.

2.5 Imaging and analysis of beating clusters in 3D scaffolds

There are several imaging techniques that are also available to be used for the imaging of hydrogels and also for the visualizing of different kinds of cells. To name the few, Confocal microscopy, Scanning electron microscope (SEM) and X-ray micro computed tomography (X-ray µCT) are some of the widely used techniques.

As far as imaging of cardiomyocytes is concerned, there are plenty of research papers available that discuss about imaging cardiomyocytes using different types of imaging modalities. However, we could not come across any article dealing with imaging of the aggregates of cardiomyocytes using Optical projection tomography. Some other methods that have been being used to image live cardiomyocytes for different purposes are being briefly discussed below.

2.5.1 Wide-field digital interferometry

Shaked NT *et al.* (2010) [35] described in detail the use of wide-field interferometric microscopy techniques for the acquisition of high resolution quantitative phase profiles of ventricular cardiomyocytes in-vitro. The whole-cell analysis of live cardiomyocytes using wide-field digital interferometry (WFDI) technique was studied [35]. The WFDI technique works by acquiring the complete amplitude and phase distribution of the light which is transmitted through the samples [35].

The advantage of using WFDI is that it captures both amplitude and phase of the cells with a single camera exposure. In addition, this technique also doesn't require any scanning or contrast agent and WFDI is especially ideally suited for the acquisition of fast cell dynamics [35]. Likewise, WFDI also makes it easier to capture the phase of the light transmitted through cells which in turn is a valuable source of information for the three-dimensional cell structure [36]. Another advantage of using WFDI is that it facili-

tates the measurements of the light transmitted through cells at nanometer scale [37] and it has also been successfully used for the research related to the kidney cells, cancer cells and red blood cells [37, 38].

However, unlike OPT technique, single-exposure WFDI technique has an issue of the inability to calculate the thickness profile of the cardiomyocytes without using numerical-based analysis tools [35]. On the other hand, with 3-D imaging of OPT, thickness profile can be easily evaluated.

2.5.2 Video image-based analysis of the single cardiomyocyte cell using digital image correlation

A very unique and non-invasive method developed by Antti Ahola, a researcher from TUT, works with the combination of a video microscopy technique and digital image correlation method. The article [2] discusses the recording of the beating of the human induced pluripotent stem cell derived cardiomyocytes with the use of a video microscopy technique. In this regard, a total number of 13 single cardiomyocytes were video-recorded at 30 frames per second rate for an exact 30 seconds. Once, the video was obtained, single cardiomyocytes were segmented to be analyzed via minimum quadratic difference, a digital image correlation method. Furthermore, time series of the vector fields of a single cardiac cell were extracted from the recorded video and contraction-relaxation dynamics of a cardiac cell were obtained after processing the vector fields. The results successfully demonstrated and proved the efficacy of a non-invasive and label-free method for the analysis of single cell beating characteristics and functionality [2].

Several other research studies [3, 39, 40] also utilized the non-invasive image correlation methods. For instance, Tomohiro Hayakawa *et al.* (2014) [39] also utilized the combination of video microscopy technique and digital image correlation method to characterize the contraction behavior of cardiomyocytes. Also in earlier study, Tomohiro Hayakawa *et al.* (2011) [40] evaluated contractile behavior of cardiomyocytes monolayer using motion vector analysis method. A similar 2-D image correlation analysis of cardiomyocytes phase-contrast images was developed and utilized by A. Kamgoue *et al.* (2009) [3]. However, the advantage of using OPT technique over video microscopy technique is its ability to image biological samples over different focal angles [6].

2.5.3 Confocal microscopy techniques

Even though confocal microscopy techniques are not directly used for the beating analysis of the cardiomyocytes but they have been used for the time-lapse imaging [18] and for the measurement of the 3-D volume of cardiomyocytes [4].

In this regard, Sakurai *et al.* (2014) [18] described the protocol of taking time-lapse images of primary rat neonatal cardiomyocytes with the use of confocal spinning disk microscope. It is further argued, in the same article, how the use of confocal spinning disk microscopy technique is instrumental for the analysis of proteins and genes' expression [18].

A quantitative study to determine the correlation between cell volume and membrane capacitance was performed with the use of fluorescence laser scanning confocal microscopy (LSCM) in combination with the whole-cell patch-clamp technique [4]. Satoh, H. *et al.* (1996) [4] highlighted the benefits of using LSCM over conventional light microscopy techniques. For instance, LSCM has higher temporal and spatial resolution at variable cell depths [4, 41]. This study used LSCM not only to assess the correlation between cell volume and surface membrane area but also to accurately measure the volume of cardiomyocytes from different mammalian species at different stages of the development [4]. In this method, a stack of images of cellular fluorescence was obtained at high resolution throughout the entire depth of the cell. After the acquisition of the stack of high resolution images, it was further processed and used to reconstruct the cell volume in 3-D [4].

However, the biggest drawback with the use of confocal microscopy is the problem of phototoxicity and photobleaching. The higher intensities of the laser cause the photo-oxidative damage to the cells [5]. On the other hand, OPT technique is totally non-destructive as it doesn't cause any damage to the cells.

2.5.4 Other methods and techniques

The previous research work done on the cardiomyocytes also included the use of atomic force microscopy (AFM) [42] to assess the correlation between the mechanical properties of the heart and the actin-myosin cross bridge cycling .The study claimed to be the first one to represent the quantitative dynamic mechanical mapping of the live cardiomyocytes. The study used AFM to determine the changes in the elastic modulus of the beating neonatal rat cardiomyocytes [42].

Kamgoué *et al.* (2009) [3], opted for the use of qualitative phase microscopy methods by using correlation-based optical flow method and differential interference contrast microscopy. However, this method was based on two-dimensional image correlation analysis of phase-contrast images of cardiomyocytes. The local cell deformations were extracted by using video-microscopy time-lapse sequences [3].

3. RESEARCH METHODOLOGY AND MATERIALS

This chapter discusses the two most important and vital aspects of how the research work has been carried out. After seeking a considerable amount of needed theoretical knowledge in the previous chapter, it should be convenient for our readers now to understand the methods that we used for the culturing of cardiomyocytes and, also, the experimental setup of the OPT technique. The previous chapter covered the theoretical aspects of the cardiomyocytes' culturing and OPT technique. However, this chapter provides a detailed account of the cell isolation and culture method, and, also, working of the experimental setup of OPT.

3.1 Cell isolation and culture

The cell isolation, differentiation and culture of cardiomyocytes take place at Heart group laboratory, BioMediTech, UTA. It meets the requirements of EU directives and national legislation. Cell handling is done under laminar flow hood and samples are kept in incubator at +37°C with atmospheric CO2 concentration of 5%. The Heart group has approval from Ethical Committee of Pirkanmaa Hospital District to do human iPS stem cell research inside the institute. The cell culture part of this work is mostly done by laboratory technician Henna Lappi and researcher Janne Koivisto.

Even though, pluripotent stem cells are considered highly capable of differentiating into all kinds of cells [43], but BioMediTech utilizes differentiation of cardiomyocytes from hESCs via END-2 co-culture differentiation method.

3.1.1 END-2 co-culture differentiation technique

In END-2 differentiation method, cardiomyocytes are differentiated from human induced pluripotent stem (iPS) cells in co-culture with mouse endodermal-like cells (END-2) and this is done with ascorbic acid and without the presence of serum [44]. The benefit of using END-2 differentiation technique is that the inducing factors for differentiation are secreted from END-2 cells. Moreover, because of the presence of differentiation inducing factors, END-2 conditioned medium is also often used in cardiomyocytes differentiation [45, 46].

Human iPS cells are cultured on mouse embryonic fibroblast (MEF) feeder cell layer in stem cell medium containing DMEM-F12 (Gibco, Life Technologies Ltd), 20% knockout serum replacement (KO-SR, Gibco, Life Technologies Ltd), 1% non-essential amino acids (NEAA, Lonza), 2mM GlutaMax (Gibco, Life Technologies Ltd), 50U/ml pen-

icillin/streptomycin (Pen/Strep, Lonza), 0.1mM β-mercaptoethanol (Gibco, Life Technologies Ltd) and 4mg/ml basic fibroblast growth factor (bFGF, Peprotech). In the beginning of differentiation, undifferentiated iPS cell aggregates containing few hundred cells are mechanically dissected from the MEFs and placed into 12-well plate on top of mitomycin-C treated mouse endodermal-like (END-2) cells in medium similar to stem cell medium, but without KO-SR, β-mercaptoethanol or bFGF. From day 14 of differentiation onwards 10 v/v-% of KO-SR is added to the medium. During differentiation fresh medium is changed to cells three times per week [47].

3.1.2 Cardiomyocytes, hydrogel and 3-D cell cultures

Beating aggregates start to appear in 15-30 days after dissociation. The aggregates are first cut and isolated from the rest of the cells by surgical scalpel under microscope and collected in 10% KO-SR cell medium. The aggregates are slightly dissociated enzymatically by treatment with three consecutive dissociation buffers, 45 min in first dissociation buffer inside incubator, 20 min in second buffer and 10 min in third buffer [47]. Then dissociation is stopped by addition of EB-medium containing KO-DMEM, NEAA, GlutaMax and Pen/Strep in same amounts as before plus 10 v/v-% fetal bovine serum (FBS, Immunodiagnostic). The aggregates have now loosened up and the tight ECM and cell-to-cell connection are more open so the cells have better ability to attach to hydrogel.

To make samples for OPT imaging, the loosened aggregates are picked up individually under a microscope into a syringe already containing desired hydrogel in non-gelated form. The mixture of hydrogel liquid and cells is carefully injected into 1mm diameter FEP (Fluorinated Ethylene Propylene) tube, with approximately two cardiomyocyte aggregates per tube. After injection the hydrogel is let to gelate around the aggregate. Control samples are made by plating aggregates to 48-well plate coated with 0.1% gelatin or containing same hydrogel as in the tubes. EB-medium is applied on top of the tube or well approximately 10 minute after gelation and fresh medium is changed two times per week. After combining cardiomyocytes with the hydrogel, the culture is checked periodically and when most of the control aggregates are beating, the tube samples are taken to OPT imaging, usually between 1-7 days after the sample preparation.

3.1.3 Preparation of hydrogels

Hydrogels are prepared with the help of stock solutions. At first, we prepared gellan gum hydrogels. By combining right amounts of gellan gum (heated to +37C) and bioamine cross-linker i.e. Spermine in a test tube, a gellan gum hydrogel was formed. Likewise, some gels were formed by the combination of gelatin and spermine. However, gellan gum hydrogels were not very ideal for the live cardiomyocytes. This led us to prepare agarose based hydrogels.

Agarose gel was prepared using Agarose Type 1 (Sigma Aldrich, UK). By combining the right amount of agarose powder in distilled water, the agarose solution can be easily obtained.

The standard agarose gel protocol was followed. We prepared agarose gels with 1% concentration. For the 1% agarose gel, 500mg of powdered agarose was mixed with 50mL distilled water. After the formation of agarose gel solutions, they were kept in an Autoclave (Tuttnauer Systec 2540 EL) and were sterilized for 20 minutes (standard time to sterilize liquids) at 121 degree centigrade temperature. All the samples were prepared in an FEP tube, having similar refractive index as water.

3.2 Sample preparation and acquisitions

For our research work, we prepared plenty of different samples at different time points. However, some of the samples were not good for the acquisitions because the aggregates were not beating due to one reason or another. However, at least 9 different samples with the beating activity were imaged and analyzed. The first two samples were prepared using gellan gum hydrogels. However, the rest of them were prepared with an agarose stock solution as it was found to have greater efficacy for the beating cells.

The acquisitions for the first three samples were taken using a customized LabView program developed by researcher Ana Soto de la Cruz who was previously working at BioMediTech. However, since the customized LabView program was originally developed and tailored for different purpose, therefore we did the remaining acquisitions with an HCImageLive program that comes along with the camera.

3.3 OPT setup

The OPT setup is presented in a simplified form in Fig 2. A sample (S) is placed in a module (tube) containing refractive index matching bath. A module, comprising of a rotational motor, is rotated with an angular step size of 0.9 degree, which results in an acquisition of 400 projection images over 360 degree rotation. Mathematically, it can be defined as 360/0.9 = 400.

The OPT system is equipped with both bright field illumination and fluorescence illumination modules. However, only bright field illumination module is being shown in figure because the fluorescence illumination module was not used for the study. The bright field illumination module (A) consists of L1 (white LED) and L2 (Telecentric backlight illuminator). On the other hand, the detection module (B) consists of an objective lens (Obj. L), a pinhole (P), tube lens (L3), and a sCMOS camera. Furthermore, the objective lens is equipped with a 5x infinity-corrected long working distance objective lens (Edmund, USA) and also has a numerical aperture of 0.14, which can be adjusted by an iris diaphragm. We also used a 10x objective lens which provided us with better

magnification and focus. The version of the sCMOS camera (Hamamatsu, Japan) used in an OPT setup is ORCA-Flash 4.0.

Furthermore, the working and construction of the OPT setup used at BioMediTech has been eloquently described, both in writing and drawing form, by the post-doctoral researcher Edite Figueiras in an article published in Biomedical Optics EXPRESS [48].

A simplified representation of an OPT system can be seen in Figure 1.

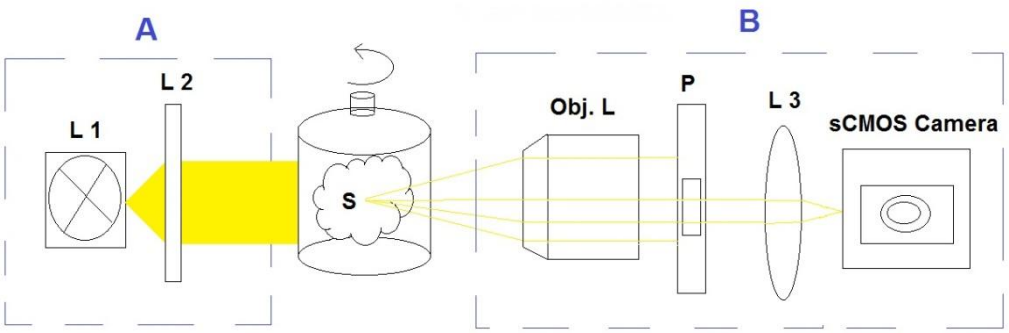

Figure 1. *Simplified representation of an OPT setup: The bright-field illumination module (A) consists of L1 (white LED) and L2 (Telecentric backlight illuminator). A sample (S) is placed inside a tube, containing refractive index matching bath and is rotated at an angular step of 0.9 degree. The detection module (B) consists of an Objective lens (Obj. L), a pinhole (P), tube lens (L3) and sCMOS Camera for the collection of images. Adopted and modified from an original source [48]*

It is also interesting to note that even though the OPT setup allows sample to be rotated at 360 degree for the acquisition of 400 images but for our research work, we didn't acquire the images with a 360 degree rotation cycle. We chose particular focal planes and completed 400-1000 acquisitions on the same focal plane. The reason for not rotating the sample over the entire 360 degree cycle is because our research work aimed at acquisitions of the beating phenomenon of cardiomyocytes and with continuous rotation of the samples, we would not be able to succeed in doing that. Hence, we only chose to rotate the samples to specific degrees to analyze the beating pattern in different focal planes. We placed our samples in distilled water bath. The placement of sample can be seen in Figure 2.

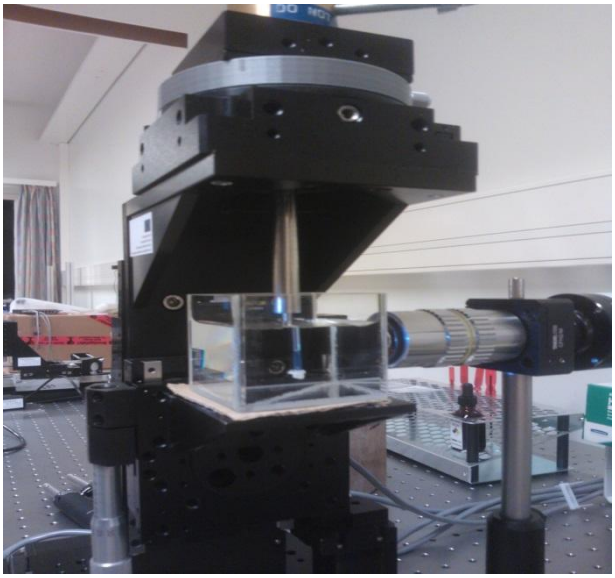

Figure 2. *A sample of cardiomyocytes placed in distilled water for the OPT imaging*

Figure 2 shows the sample immersed in a distilled water bath in an OPT setup.

3.4 Software and programs

3.4.1 Imaging and acquisitions

We used several different programs for our thesis work. The acquisition of the digital images and controlling of the OPT system was done on the computer using a LabView (Laboratory visual instrument engineering workbench) program by National Instruments, USA. Moreover, the advantage of using Labview program is that it provides a development environment where you can design the system as per the needs and requirements of the system.

The LabView program that we used for the OPT acquisitions was programmed by the researcher Ana Soto de la Cruz as already mentioned earlier. In addition to using LabView program, we also used HCImageLive for the camera control and live acquisitions. It must also be noted that HCImageLive is an imaging program that is included with the purchase of Hamamatsu camera. Moreover, HCImageLive is an easy-to-use imaging application which can be used for the real time acquisitions of biological phenomenon. It has a simple interface as shown in Figure 3.

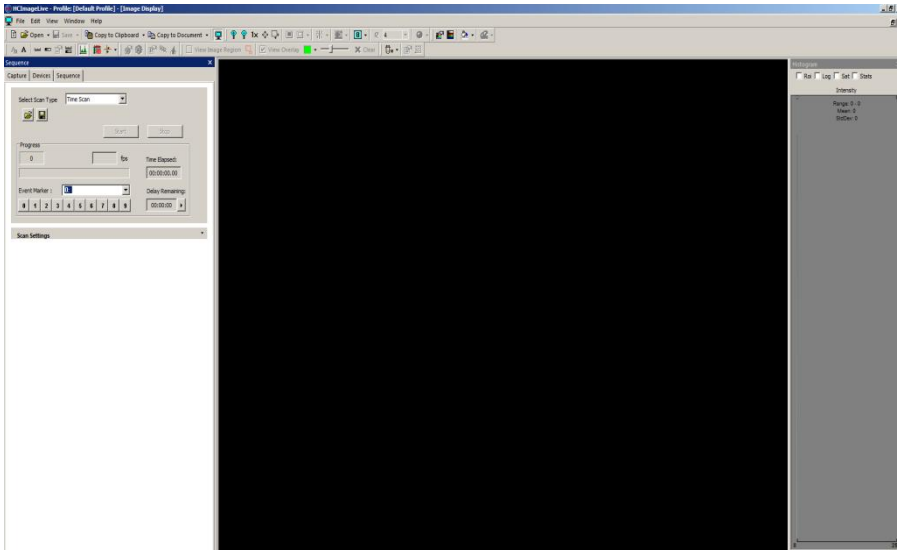

Figure 3. *The outlook of HCImageLive used for camera control and acquisitions*

We also used ImageJ to process the images that we acquired through LabView program and HCImageLive.

3.4.2 Reconstruction of videos

The reconstruction of the videos was also made possible using ImageJ which is an open source, Java-based image processing program developed at National Institutes of Health. It is specifically designed for scientific multidimensional images. We used it do the analysis and force field calculations.

The method for constructing a video using continuous acquisitions works by importing the continuous stack of images (Image Sequence) to ImageJ and then creating a video file by saving all the continuous frames in a video format (.avi). It merges all the continuous frames of images and builds a video with a very nice visualization of the biological phenomenon; beating in our case.

3.4.3 Motion analysis

We also used MATLAB program to process the images that we acquired. The motion analysis of the samples was partly done by using a special video analysis MATLAB program developed by researcher Antti Ahola [2]. The video analysis program enabled us to extract and crop the segments from the video frames that we were interested in for the analysis. The video analysis tool also enabled us to have illustrative graphs that represented the impact of the beating clusters on the surrounding gel area.

3.4.4 Sample alignment and focusing

The reason for the need of alignment and focusing can be illustrated in a better way using illustrative figures. For instance, a sample containing cardiomyocytes in an agarose-based hydrogel was put, for imaging with a 5x objective lens, in the OPT chamber. This is how the real-time live imaging looks like, as shown in Figure 4.

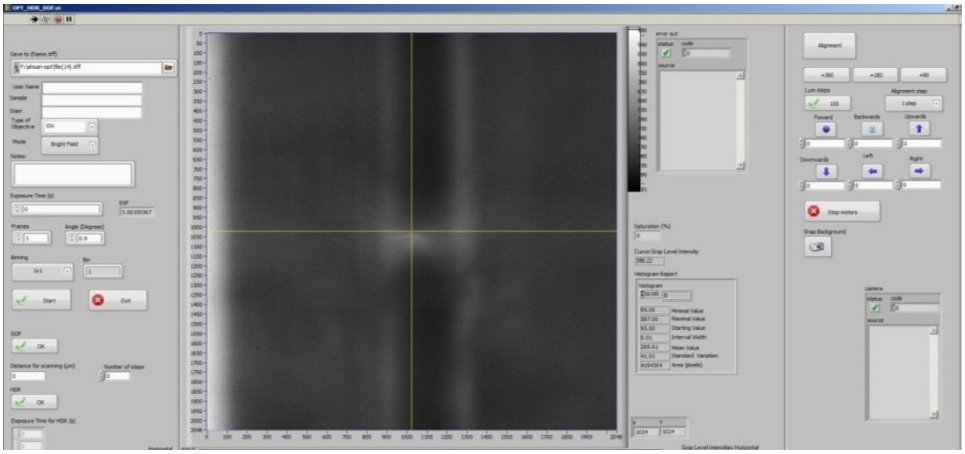

Figure 4. *Live imaging visual of the sample in a real time prior to alignment and focusing*

As it can be seen in Figure 4, we lack the suitable visualization of the sample and there is no activity to observe whatsoever. This is because of the poor focus and alignment. This problem is solved by using the alignment tools on the LabView program which are located at the top right side, beside the imaging frame. This alignment tool box, though can be seen in Figure 4 as well, has been shown clearly in Figure 5.

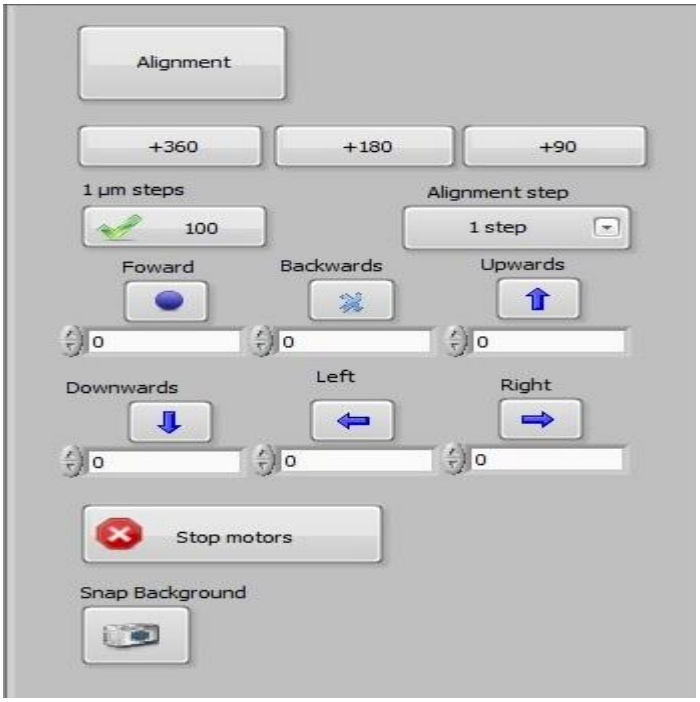

Figure 5. *Alignment tool on Labview program*

The very first button at the top called, *Alignment* is the main button which has to be clicked first because without activating the Alignment button, none of the other buttons (functions) work. In short, clicking the Alignment button allows us to use all the remaining buttons that can be seen in Figure 5. The rest of the smaller buttons are used to rotate and move the samples, align them and to obtain the right focus.

In addition, also on the left side of the LabView program is an option of putting values to *Exposure Time (s).* The ideal exposure time values also result in better visualization for the imaging.

The outlook of the sample in a real-time, as shown previously in Figure 4, was too ambiguous and vague that it was too hard to see anything inside the sample. However, after the appropriate alignment and focus, the outlook of the same sample, taken with 5x objective lens, appears to be like as shown in Figure 6.

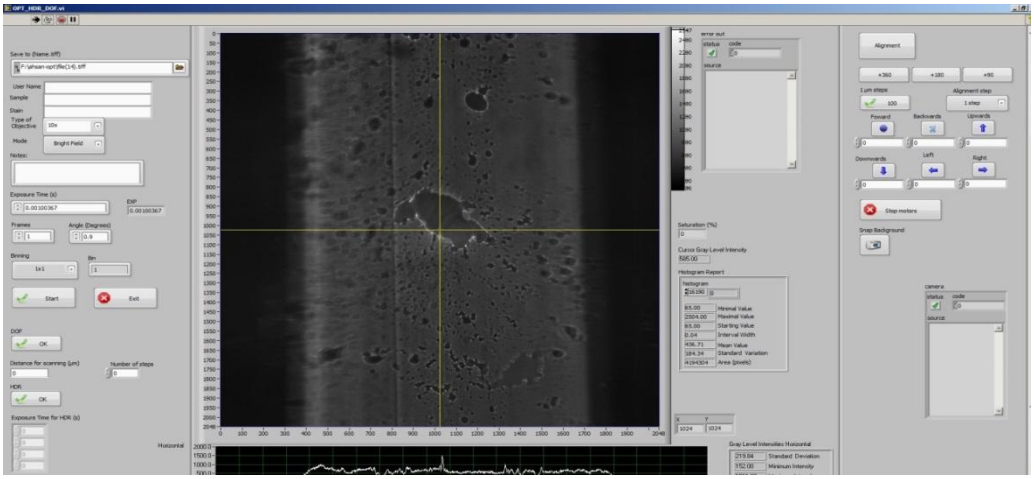

Figure 6. *Live imaging visual of the sample in a real time after alignment*

The outlook of the sample shown in Figure 6 is actually an aligned and focused outlook of the same sample shown in Figure 4. However, in Figure 4, sample is unavailable for visualization due to lack alignment and focusing. It must also be noted that Figure 6 shows the cell cluster centered in the tube but there are also other small details that can be seen within the sample. Some of the extra details, seen in all the acquisitions, come from the density variation in hydrogel. In addition, dust on camera and bubble formation in the samples can also constitute to visualization of minute details other than the cell aggregates.

Moreover, samples can be rotated and imaged at different focal angles over entire 360 degree range. This also allows to later reconstruct the videos from the images taken at different focal angles. We imaged different samples at around 90, 180, 270 and 280 degree focal planes. Moreover, selection of different focal planes is easier with visually uneven and bigger cluster since at different focal plane, visualization is distinct.

3.5 Analyses of traction forces

Once we succeeded in obtaining acquisitions of the beating cell aggregates from the OPT, we conducted analysis on the samples using the videos that we reconstructed from the acquisitions. The analysis took into account the traction forces of the aggregates and also their impact on the surrounding gel.

3.5.1 Motion analysis using MATLAB

The key feature of the MATLAB analysis part was to focus on the area of the gel that surrounds the cardiomyocytes' beating cluster. When we were able to construct the videos of the cell aggregates, we noticed that when the aggregate of the cardiomyocytes beat, they leave some impact on the gel area which is around the beating cluster.

For the qualitative motion analysis, we took different approach to have diverse illustrations of the phenomenon of beating cells and its impact on the gel.

For instance, we used the MATLAB program [2] as discussed earlier to obtain the motion signal from the gel area surrounding the aggregate. For this purpose, we chose the areas of the gel which were close to the beating aggregates and also some portions of the gel which were not as close to the beating cluster, but were still having some impact from the cells.

3.5.2 Quantitative evaluation of the traction forces

Unlike qualitative analysis, a quantitative analysis of our study focused chiefly on the beating aggregates instead of the surrounding gel area and we were able to obtain and illustrate the displacement fields and traction forces for different samples. For this purpose, we obtained velocity vectors, also called as displacement fields, from the aggregates and then we obtained the traction force values from the displacement fields. An average traction force value was also calculated from the traction force values. This was only possible using two ImageJ plugins namely, PIV (Particle image velocimetry) and FTTC (Fourier transform traction cytometry).

PIV (Particle Image Velocimetry) - ImageJ plugin

The PIV plugin on ImageJ is used to perform iterative particle image velocimetry analysis by taking into account a pair of images. It divides a pair of images into interrogation windows. Afterwards, the plugin performs cross-correlation between the sub-regions of two images and hence, measures the velocity of objects in the images [49]. The velocities or displacement are represented in terms of vectors. However, to create accurate displacement or velocity vectors for any given sample, it is essential to input a pair of images wisely. Similarly, to have an exact representation of the beating forces or displacement due to the beating forces, we needed to provide two frames of cardiomyocytes activity- one in a resting state and the other one with the contraction. For this purpose, we first used ImageJ to reconstruct 3D surface stack plots for the samples which allowed us to note the beating frames at different intervals. This way, we were able to choose one resting and one beating frame. The two frames were then imported as a stack of images on ImageJ after which PIV function was performed and we obtained the results in the form of displacement fields.

The PIV function runs iterative three passes of PIV called as PIV1, PIV2 and PIV3. All three passes of PIV represent cross-correlation for different interrogation window sizes and a better PIV resolution is attained by decreasing the interrogation window size [49, 50]. The three ideal interrogation window sizes, by default, are 128, 64 and 32 pixels.

The principle of working of PIV plugin is based on the calculation of the displacement fields through a normalized correlation coefficient algorithm in which an individual

interrogation window is compared against a larger searching window and every subsequent iteration takes into account the displacement fields obtained from the previous iteration. [51]

FTTC (Fourier Transform Traction Cytometry) - ImageJ plugin

FTTC plugin on ImageJ is used in combination with PIV plugin and it is used to reconstruct the traction forces from the displacement fields already obtained through PIV plugin. Once, we acquired PIV results, we easily availed FTTC plugin to create the magnitude of the traction forces of the cardiomyocytes [51, 52]. The FTTC plugin provides two results in a picture format; one is the vectorial representation of the beating forces and the other one is the representation of the magnitude of the force. [52].

The code for FTTC plugin was written on Java by Qingzong *et al.* (2012) [51] and the principle of working of FTTC plugin, as the name suggests, is based on the Fourier transform. The displacement fields obtained from the PIV function [49] are transformed into Fourier space and back to real time through fast Fourier technique (FFT) algorithms [53]. The PIV data file that is obtained with the use of PIV function is used as an input to FTTC function and the FTTC plugin creates a force field from the input.

FTTC function needs parameters of the material to convert the displacement fields into force fields accurately. Since, we used 1 % agarose solutions for our samples, we calculated force fields of our samples with standard estimated parameter values for 1% agarose solutions [54]. Table 2 shows the parameters that we used for the FTTC force calculations of all the agarose based samples.

Table 2. *FTTC parameters for 1 % agarose based samples*

Samples' material	Pixel size in micron (default value)	Poisson ratio	Young's Modulus in kilo-Pascal (kPa)
1 % Agarose solution	9×10^{-10}	0.5	14

Table 2 highlights the values of the parameters that we used to obtain the traction force values for all the samples. The pixel size in micron is already set by default to 9×10^{-10} micron. However, the values for poisson ratio and Young's Modulus were set, based on the characterization of the mechanical properties of the 1 % agarose gels [54].

The output file of the FTTC plugin is a text file which represents the x and y components of the traction forces in x and y co-ordinates of the data [52]. It also gives the values of the resultant magnitude force at different coordinates. The values for the traction forces are obtained in Pascal which show the contractile force exerted by the cells per unit area. Moreover, the resultant force values are automatically calculated by the plugin, based on the Pythagoras theorem and vector additions. From several traction force values for different coordinates, we chose varying traction force values for 20 different coordinate points and estimated the average traction force value based on the 20 coordinate values. The average traction force values were obtained in Pascal and were expressed in mN/mm^2.

Brief evaluation of role of temperature

In addition to the standard traction force evaluation, briefly a correlation between cardiomyocytes' traction force and temperature was evaluated. For this purpose, six samples were prepared in 1 % agarose solution but only one of the samples was found to be beating properly. However, since the temperature-based evaluation was not the chief objective of the thesis therefore we performed temperature-based experiment with one sample only.

For this purpose, distilled water bath was heated to 37 degree centigrade with the heating plate and sample was placed in a water bath for OPT imaging. Temperature was monitored with a thermometer constantly immersed in a distilled water bath. At first, real-time acquisitions were obtained at 37 degree centigrade. We kept monitoring the temperature drop and imaging acquisitions were obtained again after 5 degree centigrade drop i.e., at 32 degree centigrade. The final acquisitions were taken at 27 degree centigrade.

Videos were constructed from the real-time acquisitions and traction forces were calculated at three different temperature intervals, using PIV and FTTC plugin. Like all other samples, 20 coordinate traction force values were taken into consideration for the traction force evaluation.

4. RESULTS AND ANALYSIS

For MATLAB motion analysis, only bigger cluster of cardiomyocytes was chosen to extract the area of the gel close to the beating aggregate and to obtain the peaks of the beating from the surrounding gel area. However, regardless of the size of the samples, acquisitions were obtained for all different kind of samples and videos were constructed for all the samples. Moreover, average traction force values were calculated for the samples ranging from small sized samples to bigger clusters.

Moreover, major results and observations have been provided in this chapter while similar results and calculations have been added to ***Appendix C***.

4.1 OPT, MATLAB and traction force results

As we were able to visualize the beating aggregate using LabView software, at first we acquired several frames of the aggregate (cluster) of beating cardiomyocytes in a specific focal plane. This allowed us to make a video of beating cardiomyocytes from the images that we acquired.

The approach taken to visualize beating cardiomyocytes included taking their 400-1000 images at different focal angles, forming a video of the beating activity with the acquired images and at specific frame rates, and finally, doing the motion analysis by analyzing the specific segments around the beating cardiomyocytes using a customized video analysis tool on MATLAB [2].

However, it should also be noted that different segments of the gels tend to have different impact and activity as a result of different patterns of the beating of the cells. This is because of the fact that it is not necessary that the whole aggregate or cluster of the cardiomyocytes would be beating in a single rhythmic fashion. Therefore, the extraction of the smaller segments around the beating clusters is a nice idea to have a look on the impact caused by the beating cardiomyocytes.

For the traction force calculations, at first we used ImageJ to construct a 3D stack volume plot of the sample as it was essential to create a 3D stack plot to see the beating and non-beating frames. From these stack plots showing activity of the cells for each frame, two frames were carefully chosen to perform PIV and FTTC functions. A detailed description about these illustrative 3D volume plots have been provided in ***Appendix B*** while some traction force calculations for the values obtained through PIV and FTTC plugins have been provided in ***Appendix C***. On the other hand, to keep the thesis work

within in the decent page limits, the original images of the PIV and FTTC results have been resized to smaller sizes in this section.

4.1.1 Big cluster of cardiomyocytes

In the beginning, we constructed a video of a big cluster, cultured in an agarose gel, with 33 frames per second and 0.03 second exposure time value using ImageJ. The snapshot of our earliest observation of the beating cardiomyocytes in a specific focal plane is being shown in Figure 7.

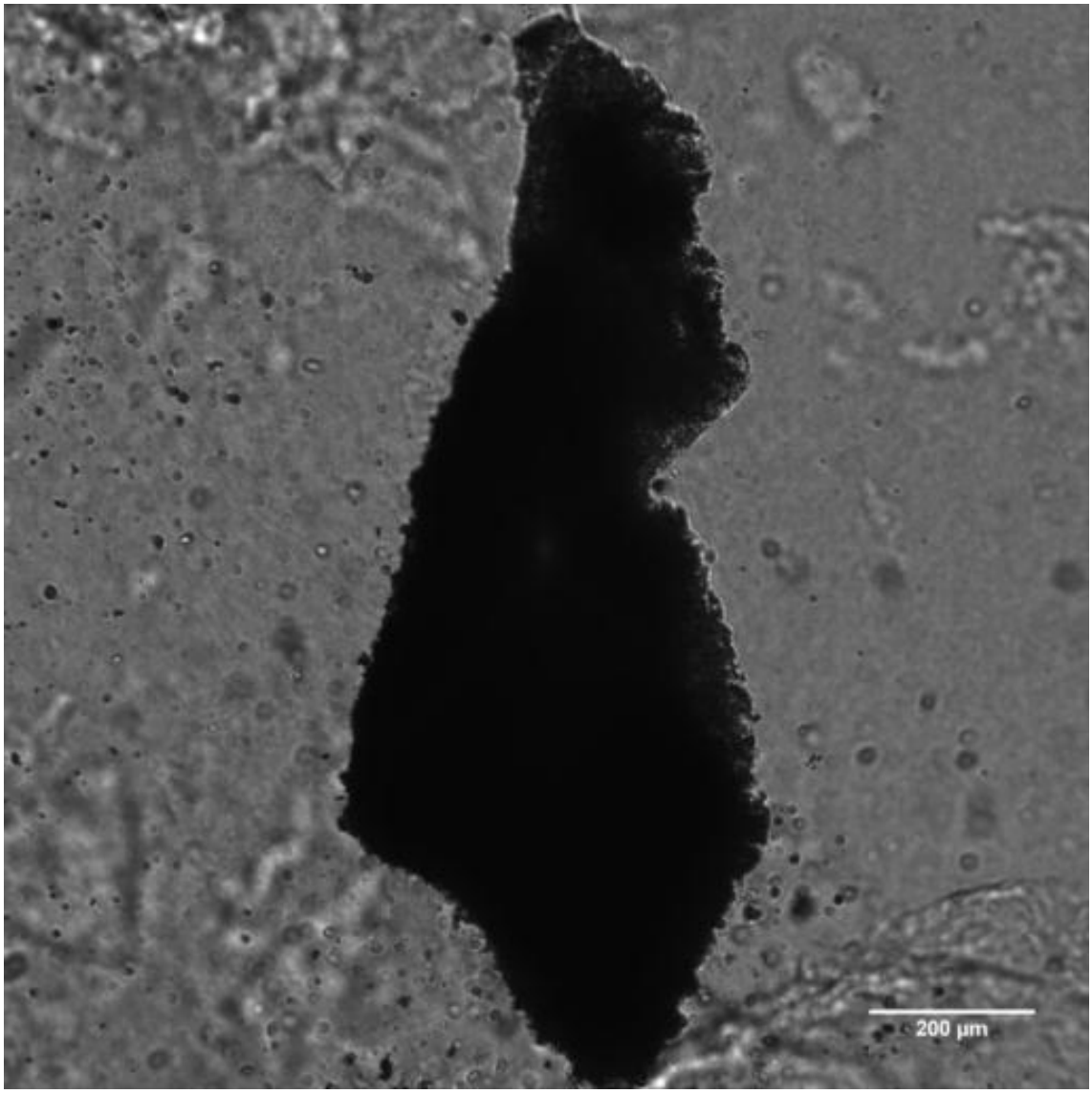

Figure 7. *Big cluster of cardiomyocytes*

Figure 7 shows the large aggregate of the beating cardiomyocytes, cultured in an agarose gel in a normally aligned position without any angular rotation.

Afterwards, the sample was also rotated at 90 degree to analyze the beating pattern at different focal plane. We also acquired 400 continuous images after the rotation and reconstructed the video from the acquired images.

Following 90 degree rotation, sample was orientated in a new focal angle as shown in Figure 8.

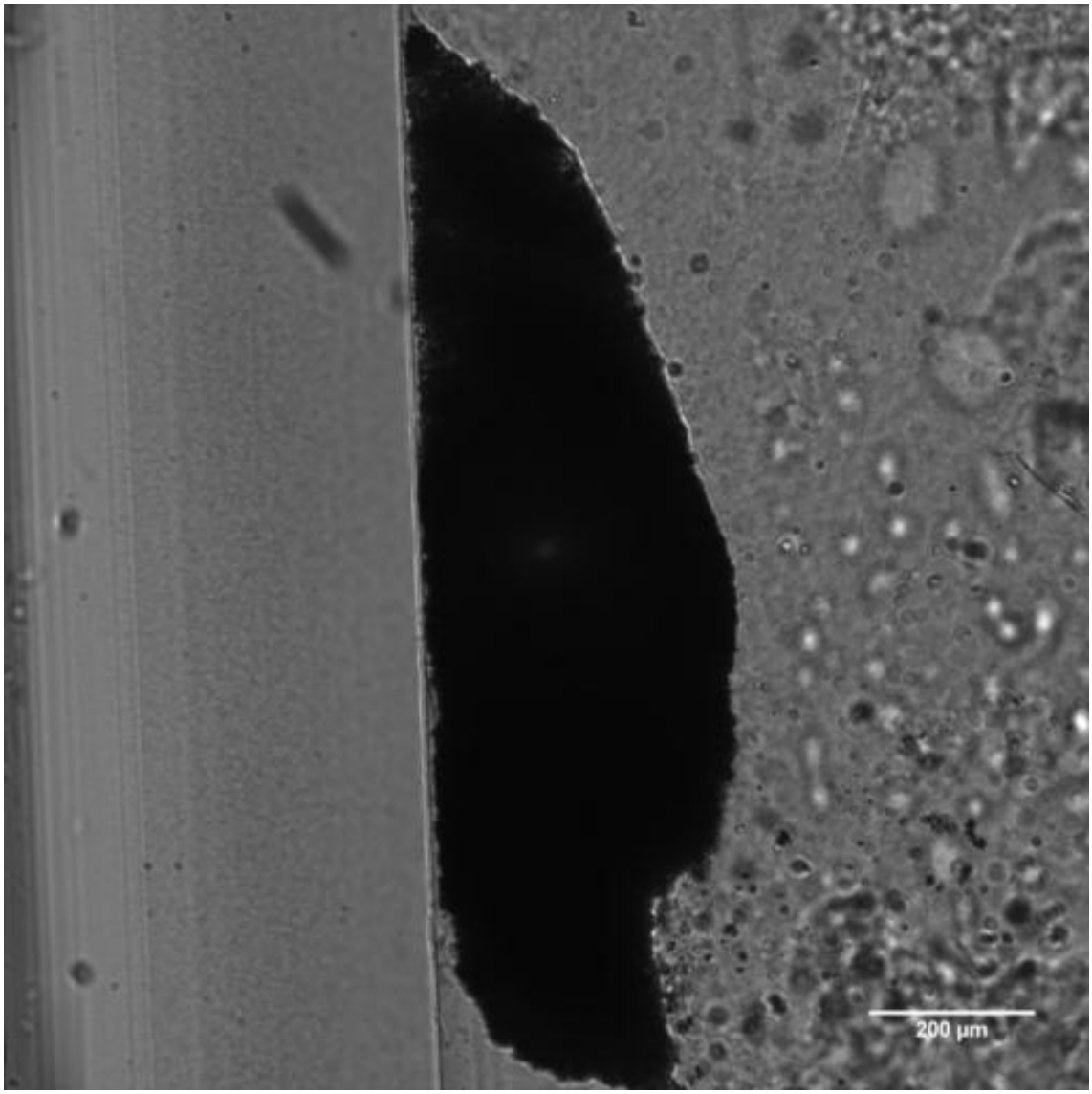

Figure 8. *Big cluster of cardiomyocytes rotated at 90 degree*

The MATLAB analysis was performed in both the focal angles. Moreover, due to the beating of cardiomyocytes, the agarose gel also has an impact of the beating due to which a similar contractile activity can be recorded in the surrounding gel. Hence, we extracted certain segments from the gel area surrounding the aggregate so as to analyze the activity of the impact caused around the cells.

The summary of the MATLAB analysis on the aggregate is shown in Figure 9.

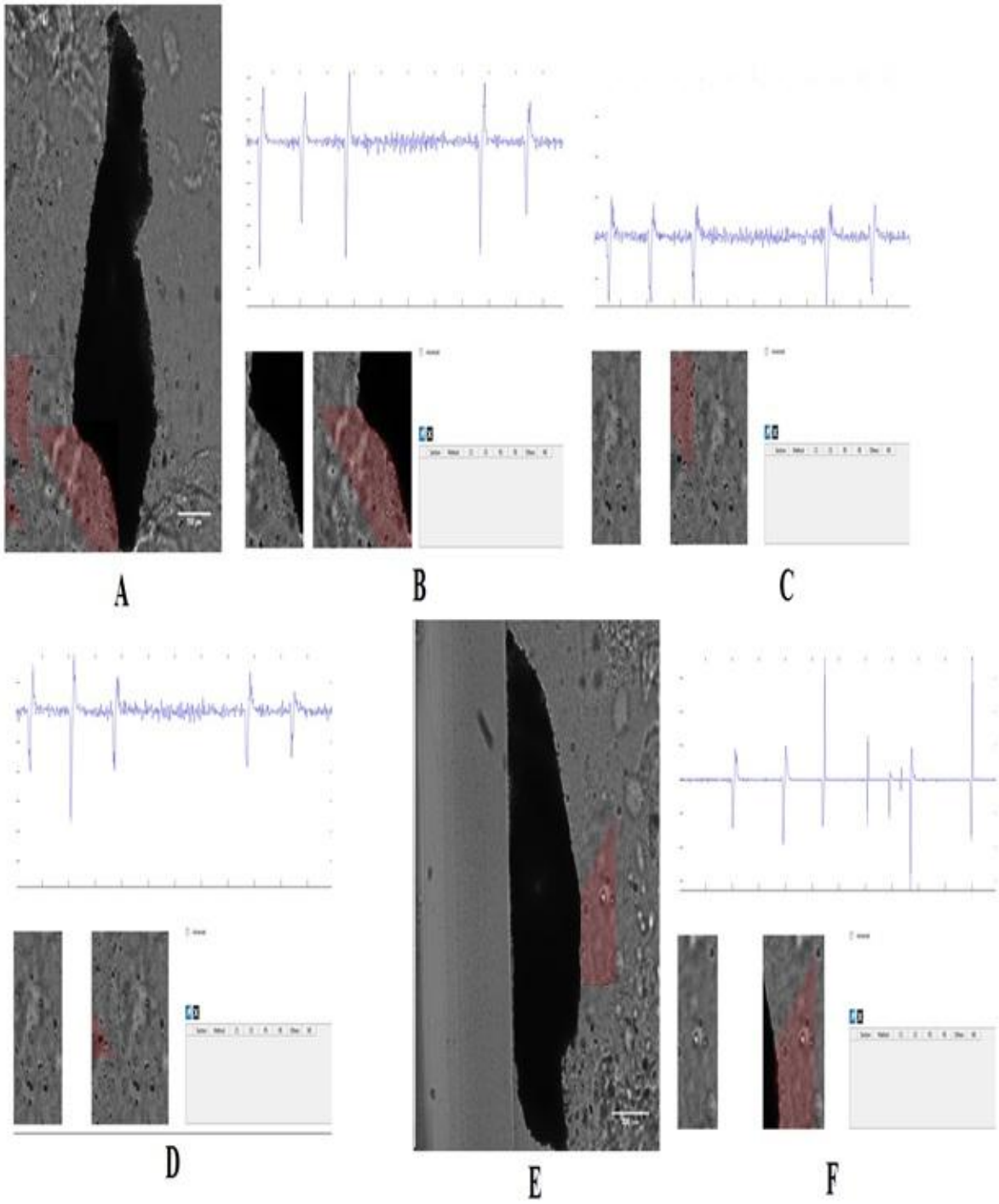

Figure 9. *(A) Big cluster of cardiomyocytes (B) Analysis on segmented portion from the bottom left of the aggregate (C) Analysis on the gel area a bit distant to the bottom left area of cluster (D) Analysis on the smaller region of gel area distant to the bottom left area of cluster (E) Big cluster of cardiomyocytes after rotation at 90 degree (F) Analysis on the gel area near the cluster shown in E.*

Figure 9 shows also the highlighted segments of the gel area that were extracted for the motion analysis. As it can be seen in Figure 9, contractile activity was observed not only in the gel area immediately close to the clusters (B and F) but also in the gel areas distant from the cluster (C and D).

Average traction force calculation for big cluster

Displacement fields were also obtained for the big cluster which confirmed the presence of velocity vectors in various directions. Thus, a big cluster showed a contractile activity almost throughout the cluster. The velocity vectors pointing in all directions can be seen in Figure 10.

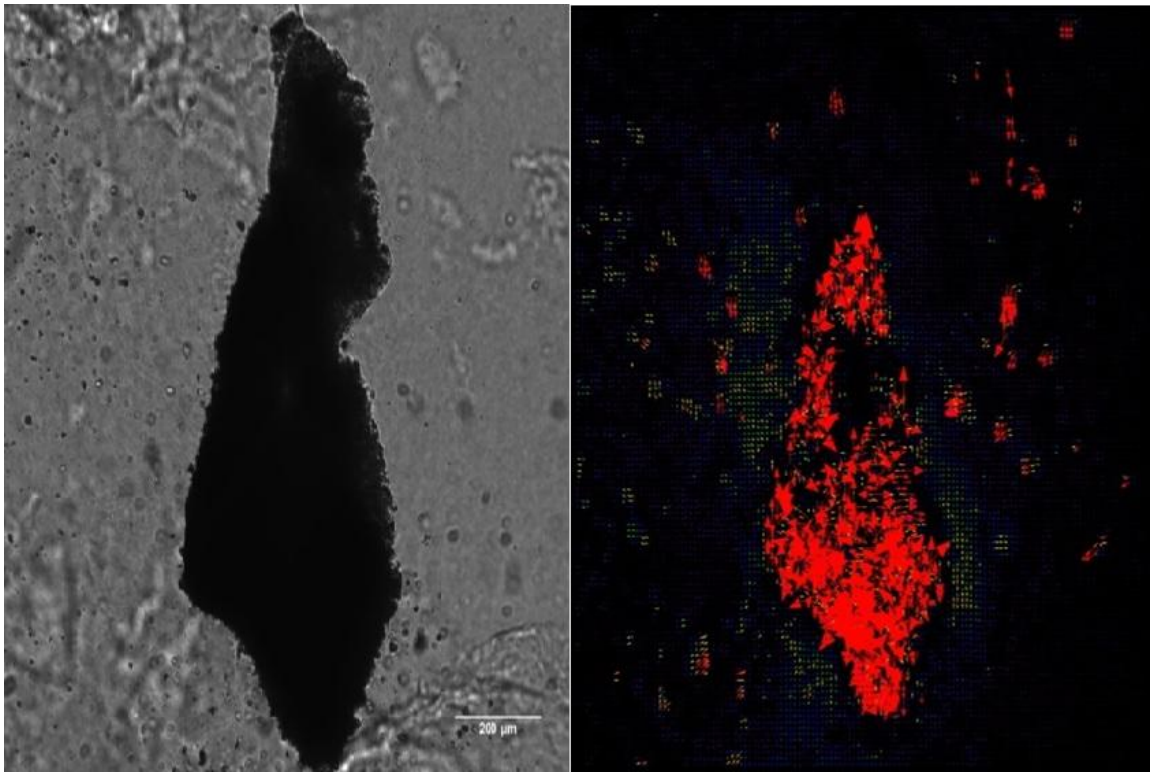

Figure 10. *A big cluster showing displacement field and indicating areas of motion*

Figure 10 shows the areas of the motion of the cells across the big cluster. An average traction force value was also calculated for the big cluster. The different values can be seen in Table 3.

Table 3. *Average traction force results for the big cluster of cardiomyocytes*

(x, y) coordinates of the data in pixels	x-component of the traction force in Pascal	y-component of the traction force in Pascal	Resultant force magnitude	Average traction force value in mN/mm²
(24.0, 24.0)	-29.845	-64.878	71.414	
(40.0, 24.0)	-48.872	-150.705	158.432	
(56.0, 24.0)	-19.850	75.790	78.347	
(72.0, 24.0)	-6.557	22.905	23.825	
(88.0, 24.0)	-12.689	-36.029	38.199	
(104.0, 24.0)	29.762	-19.402	35.528	
(120.0, 24.0)	6.402	-30.096	30.770	
(136.0, 24.0)	-54.018	15.780	56.275	**0.23**
(152.0, 24.0)	38.812	-27.441	47.533	
(168.0, 24.0)	32.342	35.003	47.657	
(1096, 1944)	402.169	-422.954	583.635	
(1112, 1944)	-29.439	363.925	365.113	
(1128, 1944)	-656.272	544.983	853.053	
(1144, 1944)	850.469	-610.311	1046.794	
(1160, 1944)	-219.464	283.801	358.758	
(1208, 1944)	75.186	193.482	207.577	
(1224, 1944)	55.019	-129.517	140.719	
(1336, 1944)	39.736	181.829	186.120	
(1352, 1944)	-101.260	-158.459	188.050	
(1976, 2024)	18.400	2.375	18.552	

Table 3 shows the values of traction forces for 20 different coordinate. The first serial number column represents the 20 different (x, y) coordinates and the next two columns show x and y components of the traction forces respectively. The resultant force magnitude values, obtained from the FTTC plugin, correspond to the traction forces values at 20 different coordinates while we manually calculated the average traction force value from the obtained resultant force values. It can also be observed in the table that different cells at different coordinates in the aggregate tend to have different traction force values. The average traction force value was calculated out to be 0.23 mN/mm².

4.1.2 Medium sized samples at different focal planes

Several acquisitions were obtained for the first medium sized sample which was rotated at different focal angles as shown in Figure 11.

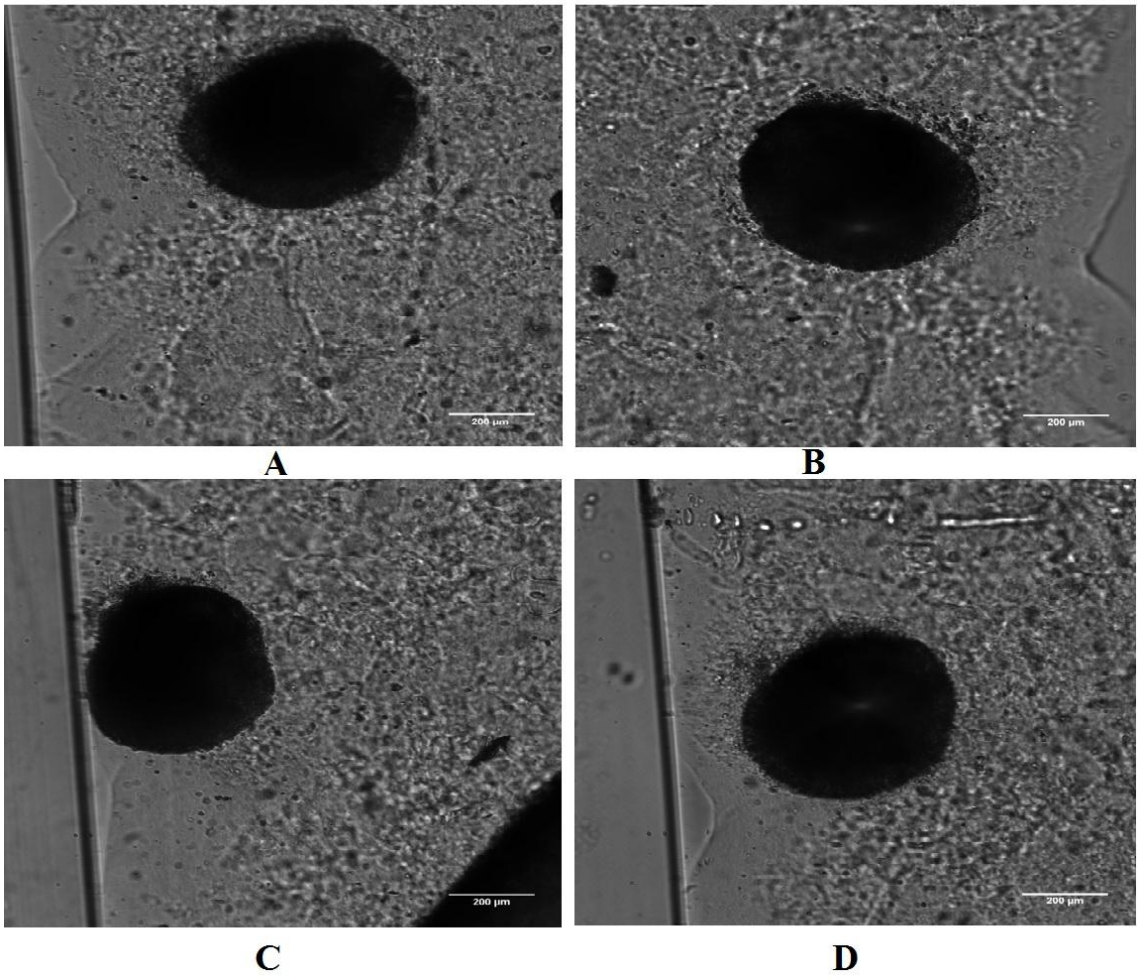

Figure 11. *(A) Sample without any rotation (B) Sample rotated at 180 degree (C) Sample rotated at 270 degree (D) Sample rotated at 280 degree*

For a medium sized sample, traction forces were calculated using PIV and FTTC functions as previously described [49-52]

Average traction force calculations for a medium sized sample

At each focal angle as shown in Figure 11, magnitude of the traction force was calculated for the aggregate. A medium sized sample exhibited different contractile behavior at different angles. A force field obtained through FTTC is being shown in Figure 12.

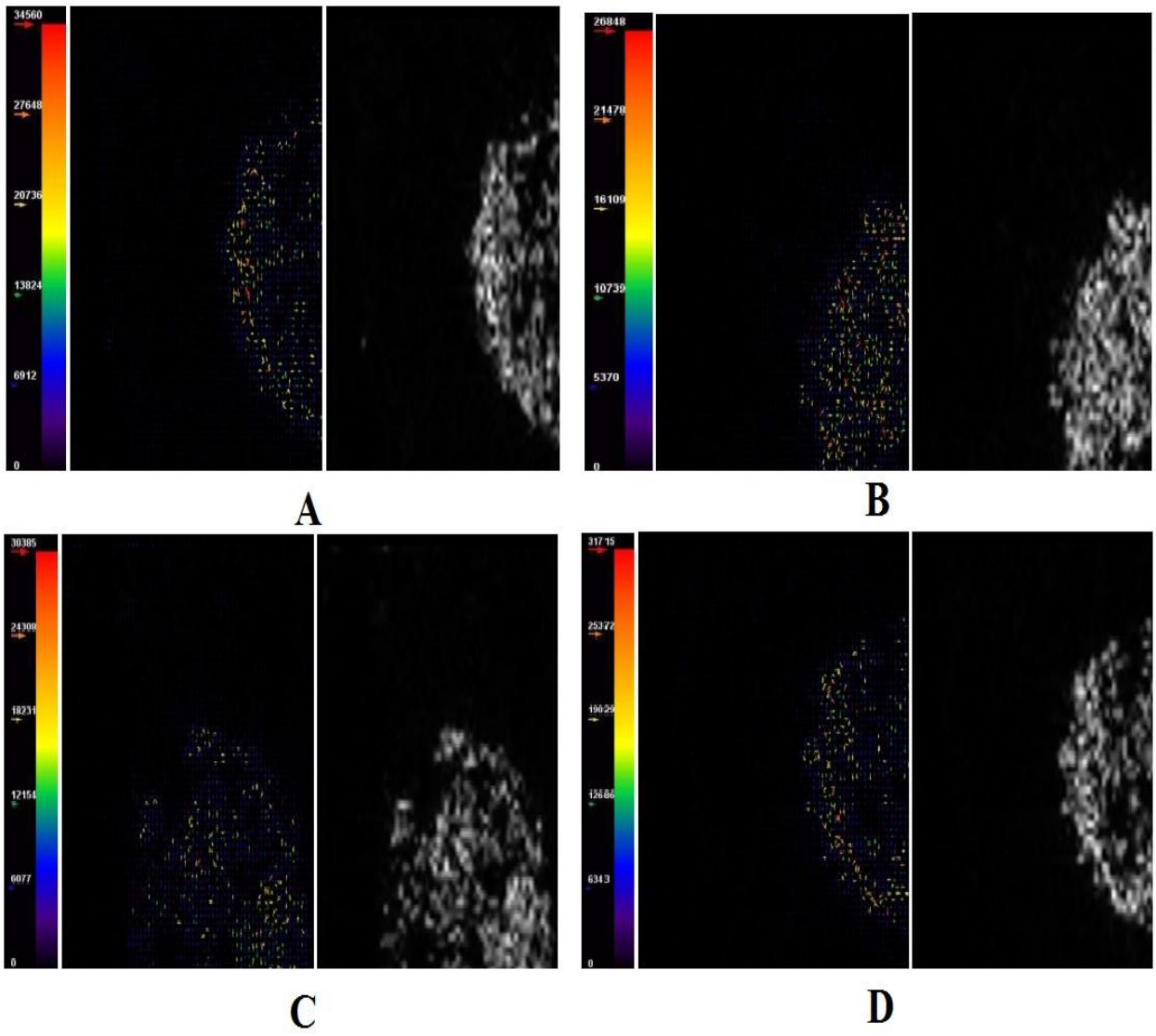

Figure 12. *(A) Force field before rotation (B) Force field after 180 degree rotation (C) Force field after 270 degree rotation (D) Force field after 280 degree rotation*

Figure 12 merely provides an illustration of the force field vectors and their magnitude. Hence, for quantification, an average traction force was calculated for the aggregate at each focal angles. The results for the traction forces, prior to any rotation, can be observed in Table 4.

Table 4. *Average traction force results for a medium sized sample prior to rotation*

(x, y) coordinates of the data in pixels	x-component of the traction force in Pascal	y-component of the traction force in Pascal	Resultant force magnitude	Average traction force in mN/mm²
(24.0, 24.0)	251.159	138.886	287.002	
(40.0, 24.0)	116.619	42.681	124.185	
(56.0, 24.0)	91.052	9.647	91.562	
(72.0, 24.0)	157.133	-265.308	308.349	
(88.0, 24.0)	239.185	-61.515	246.969	
(104.0, 24.0)	128.917	357.444	379.981	
(120.0, 24.0)	-340.936	-1033.136	1087.938	
(152.0, 24.0)	-29.791	352.865	354.120	**0.47**
(168.0, 24.0)	226.445	-374.122	437.315	
(184.0, 24.0)	94.021	-380.706	392.144	
(200.0, 24.0)	-166.044	-662.084	682.588	
(216, 24.0)	269.385	171.396	319.289	
(232.0, 24.0)	-545.221	93.416	553.166	
(248.0, 24.0)	-620.596	-568.016	841.297	
(264.0, 24.0)	407.573	-428.023	591.032	
(280.0, 24.0)	-188.944	-457.094	494.606	
(312.0, 24.0)	136.088	-512.395	530.159	
(312.0, 24.0)	167.015	-514.790	541.205	
(328.0, 24.0)	-278.776	-438.107	519.283	
(504.0, 24.0)	-245.082	-569.524	620.019	

Table 4 shows the average traction force value before any rotation. It is interesting to note that this medium sized sample showed greater average traction force value (0.47 mN/ mm²) as compared to the bigger cluster with 0.23 mN/ mm² traction force.

In addition, we also calculated the average traction force values for the medium sized sample in different focal planes. While the calculations can be seen in Appendix C, the results have been summarized and are being compared in Table 5.

Table 5. *Average traction force results for a medium sized sample at different focal angles*

	Medium sized sample without any rotation	**Medium sized sample rotated at 180 degree**	**Medium sized sample rotated at 270 degree**	**Medium sized sample rotated at 280 degree**
Average traction force value (mN/mm²)	0.47	0.14	1.03	0.31

It is interesting to note that medium sized sample showed average traction force values less than 0.5 mN/mm² at different focal planes but when it was rotated at 270 degree, it showed a higher traction force value of 1.03 mN/ mm². On combining and considering the average traction force values at different focal planes, we further calculated the overall average value of this sample which was found out to be *0.48 mN/mm²*.

Average traction force calculation for different medium sized sample

In addition, we also obtained displacement fields for another medium sized sample. The result can be seen in Figure 13.

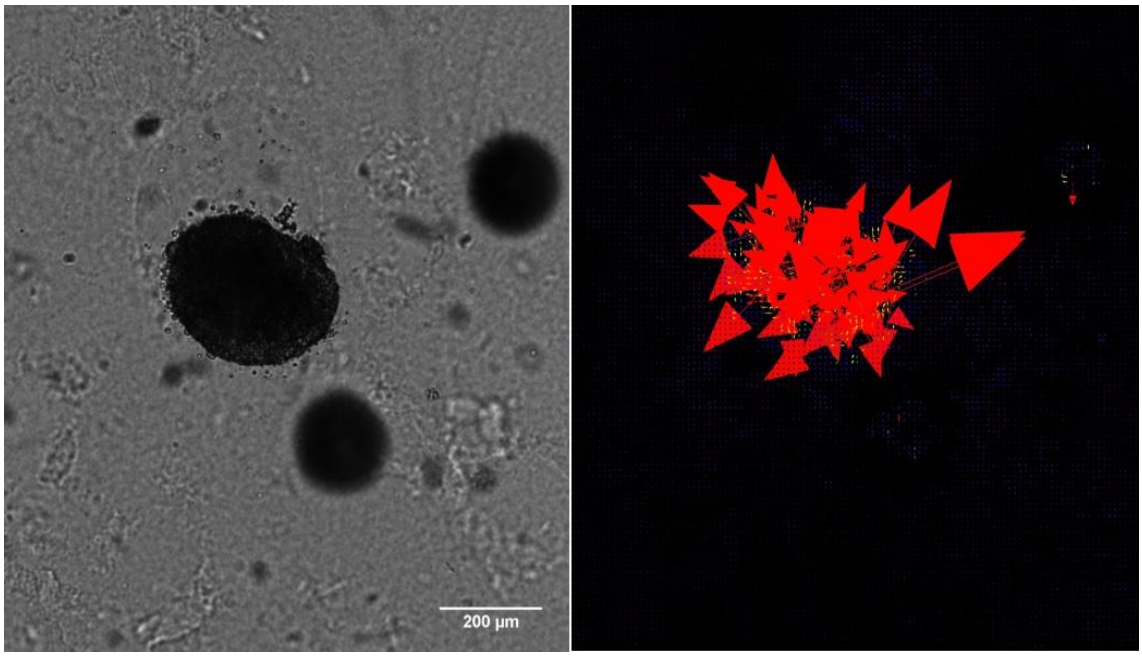

Figure 13. *Velocity vectors representing directions of motion of the beating aggregate*

The second medium sized showed displacement field vectors pointing in various directions but an average traction force value, calculated same way as previously described, was found out to be *0.20 mN/mm²* which is quite close to 0.23 mN/ mm² average traction force value of the big cluster (calculated in Table 2). The vector representation and beating pattern of the bigger cluster (shown in Figure 10) and this medium sized sample were also more or less similar.

4.1.3 Small sized samples

First small sample showed to have a very small aggregate of cells. Even though this sample had a smaller aggregate as compared to previous samples, but it was still large enough to exhibit some beating. The sample is being shown in Figure 14.

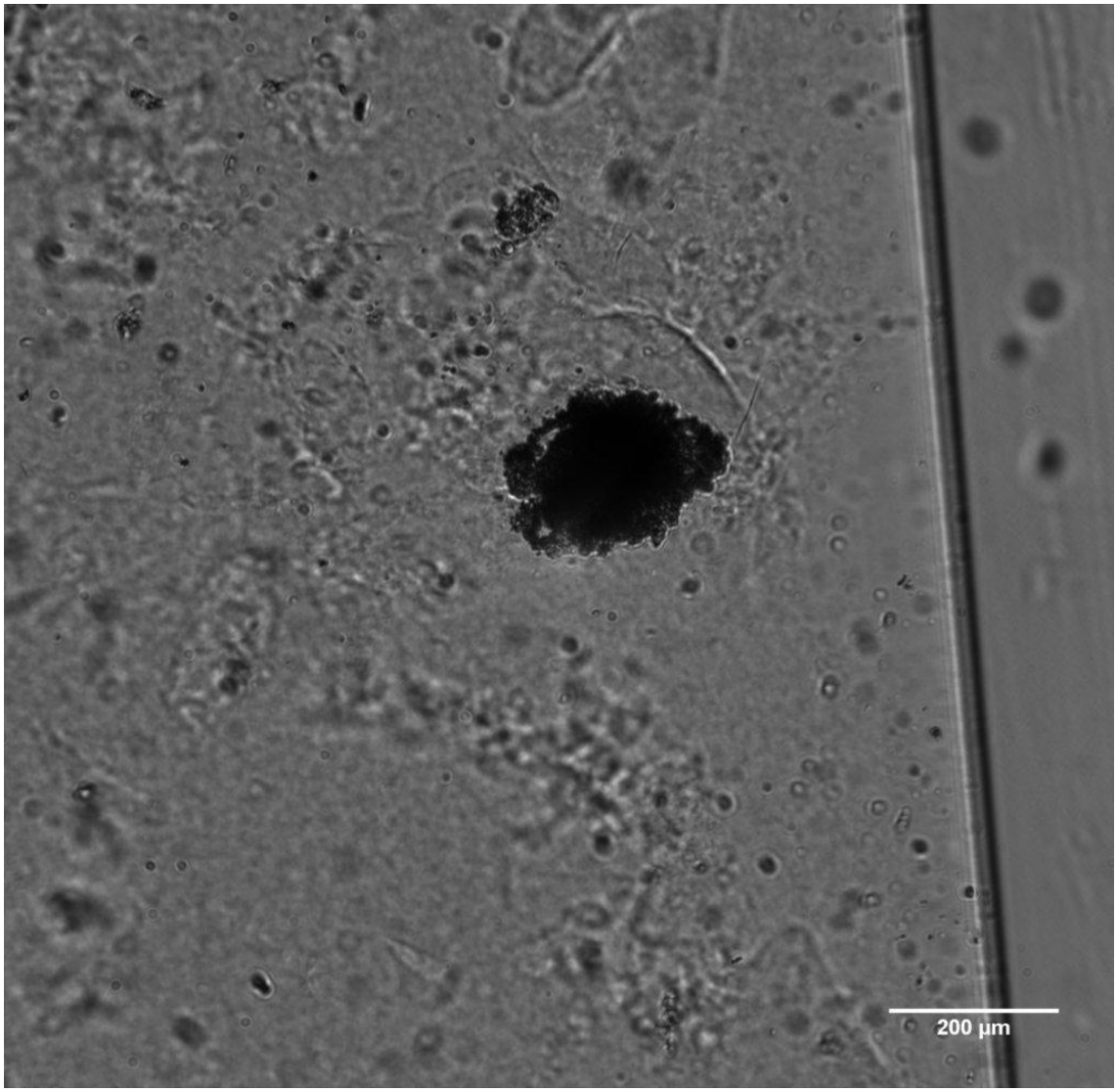

Figure 14. *Third sample of a smaller beating aggregate of cardiomyocytes*

Average traction force calculation for small sized sample

Since this sample was quite smaller in size therefore, acquisitions and construction of video were done without rotating the sample to any other focal angle. The obtained displacement fields for the sample can be seen in Figure 15.

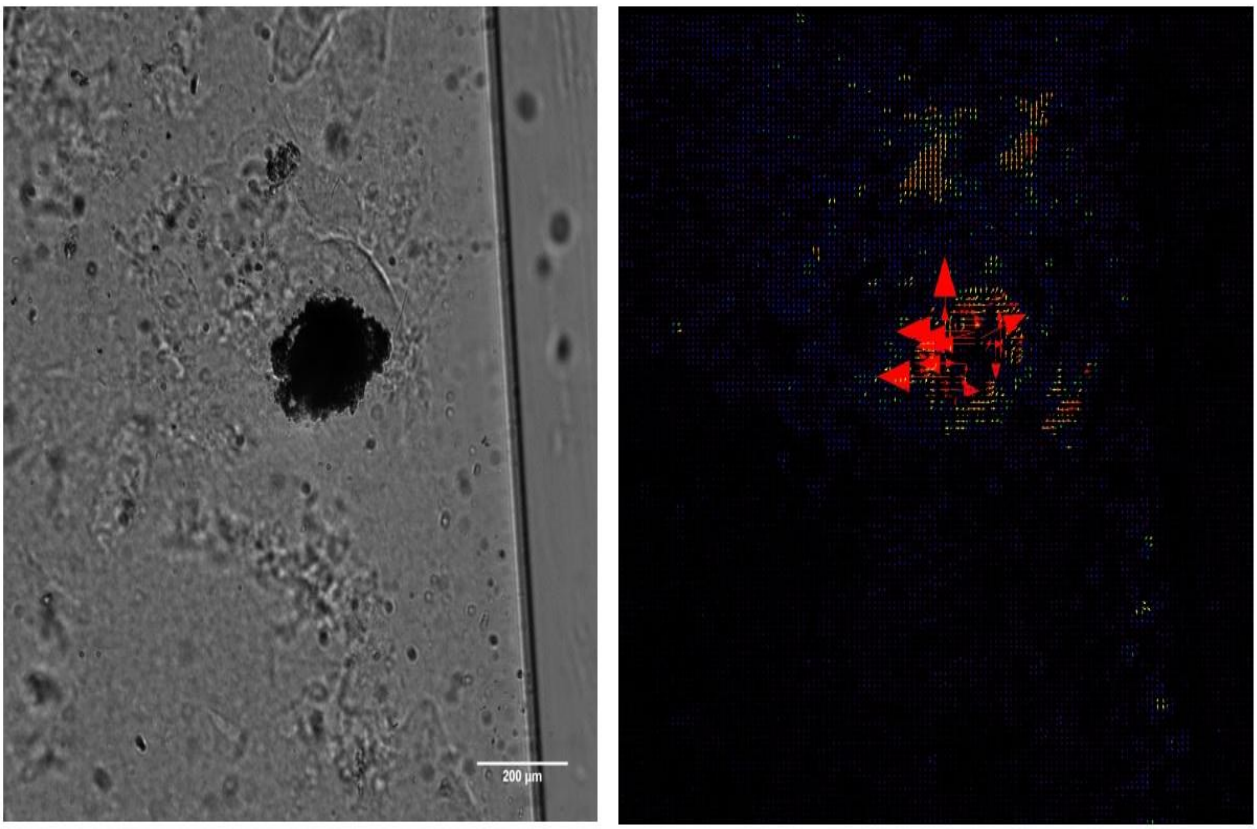

Figure 15. *Smaller sample showing displacement field vectors in different directions*

Smaller sample seemed to have lesser contractility as compared to the bigger or medium sized samples. This was also confirmed by an average traction force calculation results which can be seen in Table 6.

Table 6. *Average traction force results for a small sized sample*

(x, y) coordinates of the data in pixels	x-component of the traction force in Pascal	y-component of the traction force in Pascal	Resultant force magnitude	Average traction force in mN/mm²
(24.0, 24.0)	-5.219	-34.010	34.408	
(40.0, 24.0)	-22.801	2.263	22.913	
(56.0, 24.0)	127.210	-11.104	127.693	
(72.0, 24.0)	-26.895	-92.183	96.026	
(88.0, 24.0)	-88.427	-149.667	173.838	
(152.0, 24.0)	-24.628	-268.062	269.191	
(168.0, 24.0)	-12.694	-283.910	284.194	
(184.0, 24.0)	3.259	-136.318	136.357	**0.09**
(264.0, 24.0)	12.318	29.478	31.948	
(280.0, 24.0)	-24.498	39.499	46.479	
(760.0, 24.0)	92.272	-4.549	92.384	
(776, 24.0)	-20.778	-2.336	20.909	
(808.0, 24.0)	-15.721	-166.650	167.390	
(824.0, 24.0)	-7.673	-159.117	159.302	
(840.0, 24.0)	17.762	-136.274	137.427	
(1832, 24.0)	-17.620	-44.144	47.530	
(1848, 24.0)	6.899	-69.201	69.544	
(1880, 24.0)	14.715	30.615	33.968	
(1896, 24.0)	-5.607	-6.460	8.554	
(24.0, 40.0)	-21.499	3.153	21.729	

Table 6 shows an average traction force value for the smaller aggregate calculated to be 0.09 mN/mm² which is smaller than both the medium sized and bigger samples' values.

Average traction force calculation for different small sized sample

The displacement fields were also obtained for another small sample. The second smaller sample appeared to have more beating cells than the first smaller sample but it also showed lower contractility as compared to bigger samples. The displacement fields of this sample can be seen in Figure 16.

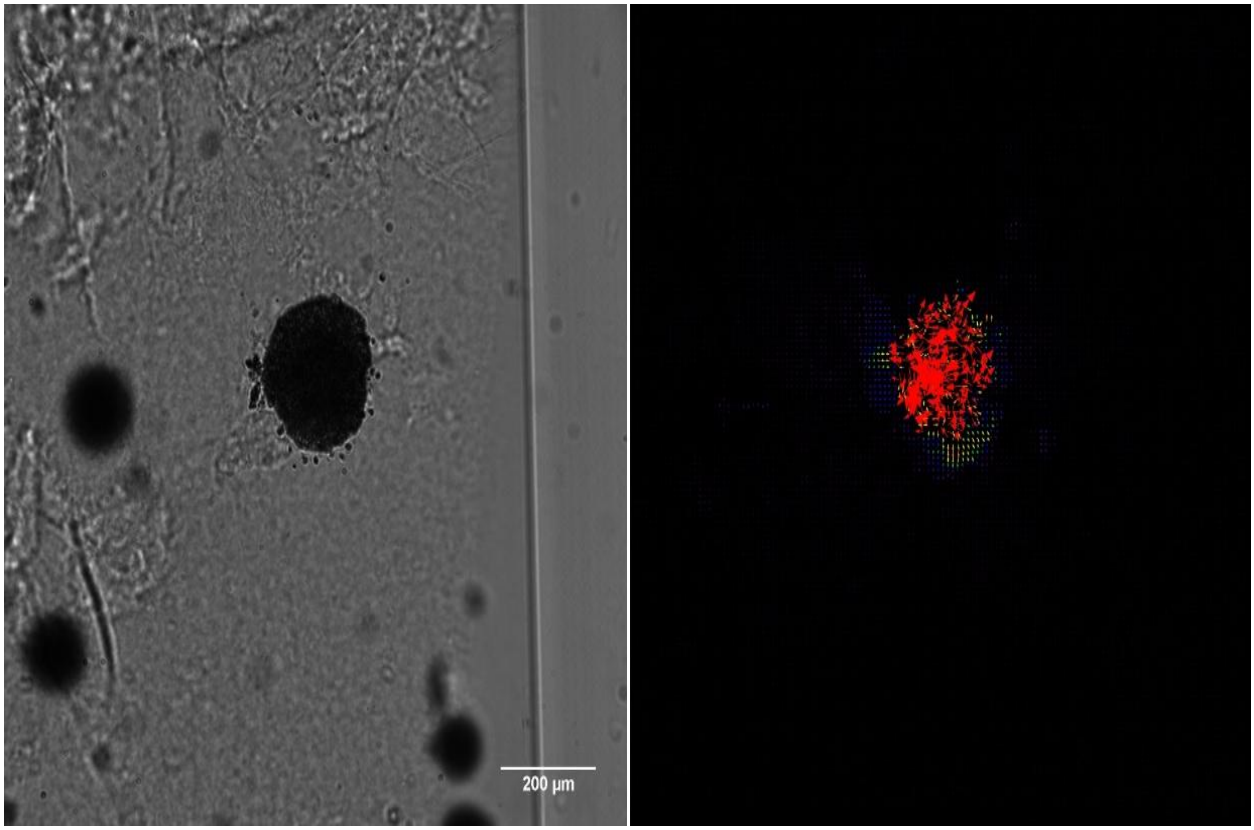

Figure 16. *Small aggregate showing indicating smaller velocity vectors*

While comparing Figure 15 and 16, it can be seen that smaller aggregate which appeared to have more cell mass showed greater number of velocity vectors due to large number of cells. However, an average traction force value for this second smaller sample was found out to be *0.07 mN/mm²* which is quite close to the first smaller sample with *0.09 mN/mm²* average traction force value.

4.2 Temperature-based evaluation of average traction force

A sample that was used to evaluate the temperature dependence can be seen in Figure 17.

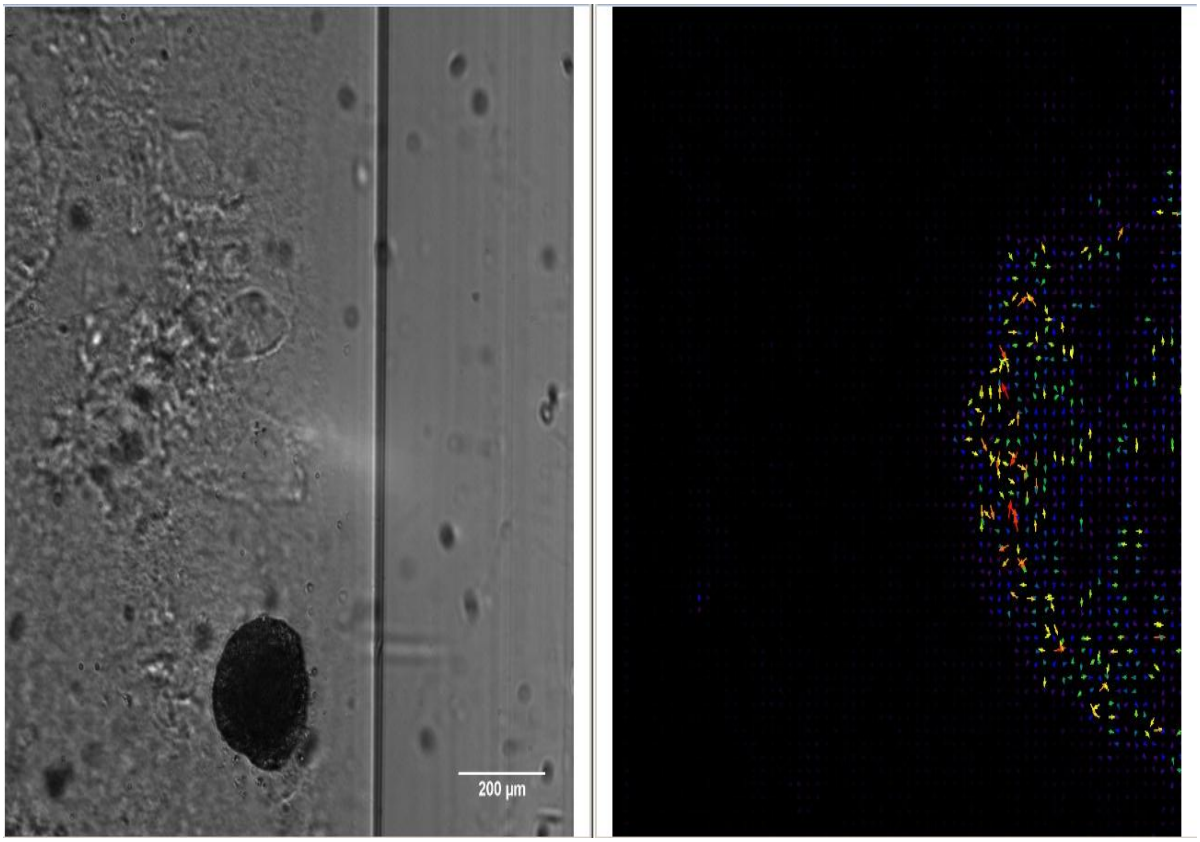

Figure 17. *Sample used for temperature-based evaluation.*

Figure 17 shows the sample that was used to evaluate briefly a correlation between temperature and cardiomyocytes' traction forces. On the right side of the figure can be seen a force field that was obtained at 37 degree centigrade.

While the calculations for the average traction force values obtained from 20 different coordinates can be seen in Appendix C, the final results of the average traction force values can be seen in Table 7.

Table 7. *Temperature-based average traction force results*

Temperature in degree Centigrade	**Average traction force value in mN/ mm²**
37	0.56
32	0.55
27	0.42

Table 7 shows the average traction force values obtained at three different intervals. At 37 degree centigrade, an average traction force value was approximately calculated to be 0.56 mN/ mm². At 32 degree centigrade, there was only a little drop in an average traction force value with the value falling from 0.56 mN/ mm² to 0.55 mN/ mm². However the final readings, at 27 degree centigrade, were found to be quite lower (0.42 mN/ mm²) as compared to an initial average traction force value (0.56 mN/ mm²) at 37 degree centigrade.

5. DISCUSSION AND CONCLUSIONS

This chapter aims to discuss in brief and to the point, all the research work that was carried out during the thesis work. In addition, few conclusions, based on the observation and results, have been drawn in this chapter.

The thesis work aimed to analyse the three dimensional (3-D) culture models of cardiomyocytes and to acquire the images of these cultures using the Optical projection tomography technique. The imaging and analysis of cardiomyocytes was found to be more popularly done with techniques other than OPT. The apparent reason for the lack of pre-existing work on the use of OPT for cardiomyocytes is probably because of the fact that OPT is optimized for imaging a bit larger and static samples such as tissues, organs and embryos etc. [6]

5.1 Cell culturing method and hydrogel selection

Cell culturing is the process of growing cells under the controlled conditions which can be done with both 2-D cell cultures and 3-D cell cultures. The preference of using three dimensional cell culture models over two dimensional cell culture models has already been justifiably explained in the Chapter 2. The key points of which are being emphasised here. The 2-D cell culturing technique is an old and traditional way of culturing cells as a monolayer using Petri dish or flask as a container and synthetic mediums are used to provide the vital nutrients to the cells. The cells tend to grow inside the 2-D petri dish or a flask and the process is regulated at a body temperature i.e. 37 degree centigrade.

The 3-D cell culturing method, on the other hand, is relatively new and widely used technique nowadays. In a 3-D cell culturing method, cells are allowed to grow in all three dimensions in a bioreactor or a 3-D petri dish and 3-D cell culturing methods have also been found to be more viable and useful over 2-D cell cultures [20, 21]

In our research work, the very first stage was to be successfully able to culture 3-D cardiomyocytes in a hydrogel. At first, we decide to begin with culturing cardiomyocytes using gellan gum based hydrogels but they did not turn out to be any instrumental in the cell culturing process. The reason why we chose to begin with gellan gum hydrogels is because they are easily accessible because of their low price and they also have high biocompatibility. Moreover, we also wanted to test the efficacy of Spermine which acts as a cross linker in a hydrogel. However, cardiomyocytes didn’t seem to fit well in the gellan gum hydrogels since no beating activity was recorded. This led to the idea of

experimenting with the use of Agarose based hydrogels for the cell cultures. The results from the preliminary experiments with agarose based gels were quite promising. Thus, we made 1% agarose gel solutions. Hence, we were finally able to image the 3-D cultures of live cardiomyocytes. We also realized that Gellan gum hydrogels need to be tailored to be used with cardiomyocytes. In this regard, research studies are taking place in Heart group, BioMediTech, UTA.

Even more, once we also prepared two different batches of cardiomyocytes, each, with three different mediums; one with the gelatin coating, the other one with the agarose solution and the third one directly placed inside the cell culture medium and then to the FEP tube. Both the batches showed that cardiomyocytes only seemed to be beating out in the agarose solution. There was no beating activity recorded with the gelatin and neither with the culture medium. Besides, the culture medium was dribbling out of the FEP tube since it would not gelate like a hydrogel. However, these tests were done as an experimentation to see the results.

Hence, from this cell culturing process, we can at least conclude that agarose-based hydrogels are more suitable for 3-D cell cultures of cardiomyocytes as compared to gellan gum hydrogels. However, gellan gum hydrogels need to be optimized and tailored to obtain similar results like agarose-based hygrogels.

5.2 OPT results; advantages and discrepancies

To our understanding and research, plausible reasons why researchers previously didn't take much interest in the use of OPT for imaging cardiomyocytes are being highlighted below.

- OPT is optimized mainly for the analysis of non-moving samples. On the other hand, the beating of cardiomyocytes is associated with the movement analysis.
- Optical microscopy and other imaging techniques have already been shown to be well-suited for the imaging of cardiomyocytes [2, 3, 34, 35, 36].
- With other techniques, it is quite convenient to use objective lens ranging from 20x to even 40x. On the other hand, we imaged our samples using 5x-10x objective lenses. The greater the resolution, the better images we can acquire but it comes with a compromise on the field of view as it tends to get smaller with higher magnification objective lenses.
- With OPT, it is quite difficult to observe the beating of small individual cardiomyocytes.

Based on the above mentioned points, it was quite challenging for us to carry on with the idea of using OPT for the acquisition of the images. However, at the same time, these challenges are what made this thesis work original and novel.

Even though, we were able to do the acquisition of the images of cardiomyocytes' clusters but in the beginning, we encountered acquisition problem using LabView program. The customized LabView program was encountering random delay during acquisitions which meant that there could be a lack of synchronization between the acquisition results and the actual beating rate of the cells. That problem arose because the customized LabView program was not tailored to take the acquisitions of the beating clusters. However, we were able to fix that problem with the use of HCImageLive program.

The contrasting features of pros and cons of our approach towards using OPT, for the imaging of 3-D cell cultures of cardiomyocytes, have been summarized in Table 8.

Table 8. *Advantages and disadvantages of our research approach*

Advantages	Disadvantages
Acquisition of real-time images using HCImageLive and reconstruction of videos using ImageJ is also possible	Acquisition lag with the customized LabView program.
Good focus and field of view with the use of 10x objective lens	Other imaging techniques have higher resolution
Good visualization on different focal planes	Complete 360 degree rotation not possible due to beating cells.
Suitable for clusters and aggregates of cardiomyocytes	Not very ideal for smaller single cells

5.3 PIV, FTTC and traction force calculations

The PIV and FTTC results were quite instrumental in the illustration of the displacement fields and force field. In addition, they were also helpful in calculating the average traction force values for the samples.

The good thing was to be able to calculate the average traction force values for the beating aggregates of all different sizes. This also allowed us to compare the average traction values for different samples. However, it must also be noted that since our calculations were based on the traction force values obtained from only 20 different coordinates therefore, an average traction force value that we calculated for each sample was an approximate traction value instead of the exact traction value.

Moreover, a summary of the chief results has been provided in Table 9.

Table 9. *Summary of the main results*

Samples	Number of cells	Diameter in µm (for medium and small sized aggregates)	Average traction force value in mN/mm²
Big cluster	Approximately in thousands	Not applicable for big cluster	0.23
First medium sized cluster	Few hundreds to thousands	320	**0.48**
Second medium sized cluster	Few hundreds to thousands	300	0.20
First small sized sample	Most likely in hundreds	200	0.09
Second small sized sample	Few hundreds to thousands	220	0.07

Table 9 shows also the cell count (number of cells in an aggregate) and diameter of the medium and small sized samples. Since it is not very easy to calculate the exact cell count therefore, the approximate values have been provided. Moreover, since the big cluster was not round in shape therefore, no diameter value was calculated. Also, for the first medium sized sample, the average traction force value has been provided instead of different values at different focal angles.

From the results, it was found out that average traction force value of the first medium sized sample was the highest amongst all. However, big cluster and second medium sized cluster showed similar values. On the contrary, both the smaller clusters showed smaller traction force values than the medium sized and big sized clusters.

5.4 Qualitative versus Quantitative analysis

The chief objective of this research work was about the imaging and analysis of 3D aggregates of cardiomyocytes using OPT technique. This, itself, was quite a task since there was no data available in this regard and the prevalent idea in the scientific community about imaging the cardiac cells is to image them with the imaging techniques other than OPT. We also wanted to evaluate the efficacy of OPT as a tool to image 3-D cell cultures.

Since, the aggregates of cardiomyocytes were plated in 3D hydrogels, therefore it was also a good idea to obtain motion signals from the gel area surrounding the aggregate and to compare the impact of the beating cluster through different signals obtained. We obtained motion signals from the MATLAB video analysis tool [2] and since the motion analysis was purely qualitative, we did not have any parameters or values for our obtained signals. However, the MATLAB analysis illustrated the impact of the contractile activity of the cells in the clusters.

While the quantitative analysis enabled us to obtain the approximate average traction force values, but the calculations were based on 20 force values at 20 different (x, y) coordinates. It was impossible to consider all the coordinates and all the values from the aggregates since there were several hundreds of values at different coordinates.

In addition, if we were to perform even more quantitative analysis, we would require performing AFM to do the beating measurements and that itself is quite a work which alone could easily account for the main objective of the Master's thesis. Also, AFM is optimized for the individual single cardiomyocytes and not for the beating aggregates in a hydrogel. Also, AFM results could be prone to errors while using with soft materials such as hydrogels. Hence, considering the chief objective of our research work i.e., acquisition and imaging of the clusters of cardiomyocytes with the OPT, doing more experiments with the AFM would have been impossible and also, beyond the scope of Master's thesis.

In addition, the quantitative measurements of even single cardiomyocyte cells using AFM requires trained personnel to operate on the AFM and there were currently no authorized personnel available to help with the AFM. Besides, even with the trained personnel, AFM measurements on cardiac cells are not very easy to perform and there can be a lot of difficulties encountered during the whole process.

We were also informed that the quantitative measurements of the single cardiomyocytes using AFM [55] were already performed few years ago by Indradumna Banerjee at TUT (Tampere University of Technology). Moreover, transducer based methods were also reviewed besides performing atomic force microscopy on single cardiomyocyte cells [55].

For our study, in both qualitative and quantitative analyses, we simplified the results in the forms of comparative figures and descriptive tables. We also carefully marked the areas of the gel around the beating clusters which we chose for the qualitative analysis. On the other hand, the quantitative measurements, having results in the form of numerical values, not only approximated the average traction force values but also provided illustrative displacement and force fields.

5.5 Temperature based evaluation of average traction forces

Even though the results obtained from the temperature-based traction force evaluation showed the drop of traction force values with the falling temperate but since our experiment was based merely on one sample, therefore we will not derive any conclusions based on the obtained results.

6. FUTURE PROSPECTS

The thesis work enabled us to experiment, explore and deduce some useful inferences in terms of the use of OPT technique for the imaging of cardiomyocytes clusters. Based on the successful acquisition of images and translation of images into videos, it can be stated that it is quite possible to acquire the images of live cardiomyocytes aggregates using OPT system. However, the only requirement is that cells should not be too small or in other words, individual cells. Rather, it is quite convenient and viable approach to image the aggregates or clusters of cardiomyocytes. It gives a good picture of the whole beating cluster in a gel.

First and foremost, this thesis work has established the possibility of using OPT system in the future as well for any kind of research with the clusters of beating cardiomyocytes, especially at BioMediTech.

During the cell culturing process, we came up with the conclusions that agarose based hydrogels were best suited for the live cardiomyocytes aggregates. However, we also realized that with certain modifications, gellan gum hydrogels could also compete with agarose based hydrogels for the culturing of cardiomyocytes. In short, besides imaging experiments, it has also made us think about trying different culturing methods and techniques using both gellan gum and agarose based hydrogels. In the future, gellan gum based hydrogels can be modified and tailored so as to increase their efficacy for their use with the cardiomyocytes.

The current progress and success with the thesis work has also opened the doors for the novel and possible improvements. For instance, it is also quite possible to make a customized LabView program that could enable the acquisition of the images in quite a real-time frame without any lag in the acquisitions. Likewise, there are many possibilities of creating improvised versions of LabView programs that could work better with the OPT system. However, that would be an additional thing to do since HCImageLive also works fine with the real time acquisitions.

One important thing about the average traction force calculations is that it can be approximated in even better way if more values are taken into account. Therefore, it is also quite possible to optimize the average traction force calculation methods in the future. Also, for better estimations and quantifications, fluorescent beads can be added to the samples since PIV and FTTC plugins work well with the fluorescent beads [49, 52]. Besides, the hypothesis of the dropping traction force values with the falling temperature can be evaluated further with more similar experiments in future.

Also, while reviewing other methods that are used for cardiomyocytes imaging, WFDI technique was found to have a lot of advantages over other traditional methods. Therefore, we would like to do the imaging of the beating aggregates with WFDI technique as well.

Nevertheless, after the successful acquisition of images and videos with the OPT system, other researchers working at BioMediTech have also contacted us and provided us with their own samples of cardiac cells to do their imaging with the OPT system. With a diverse range of cardiac cells, cultured and processed differently, it would be very interesting to perform different kind of experiments and have some more conclusions and results in future.

REFERENCES

[1] Winitsky SO, Gopal TV, Hassanzadeh S, Takahashi H, Gryder D, Rogawski MA, et al. (2005) “Adult Murine Skeletal Muscle Contains Cells That Can Differentiate into Beating Cardiomyocytes In Vitro”. PLoS Biol 3(4): e87. doi:10.1371/journal.pbio.0030087

[2] Ahola A., Kiviaho A.L., Larsson K., Honkanen M., Aalto-Setälä K., Hyttinen J. (2014 Apr 7;13:39) “Video image-based analysis of single human induced pluripotent stem cell derived cardiomyocyte beating dynamics using digital image correlation.” Biomed. Eng. Online. doi: 10.1186/1475-925X-13-39.

[3] Kamgoué A., Ohayon J., Usson Y., Riou L., Tracqui P. (2009) , “Quantification of cardiomyocyte contraction based on image correlation analysis,” Cytometry A 75(4), 298–308.10.1002/cyto.a.20700

[4] Satoh, H., Delbridge, L. M., Blatter, L. A., & Bers, D. M. (1996) “Surface:volume relationship in cardiac myocytes studied with confocal microscopy and membrane capacitance measurements: species-dependence and developmental effects”. Biophysical Journal, 70(3), 1494–1504.

[5] Claudette M. St. Croix, Stuart H. Shand, and Simon C. Watkins (December 2005) “Confocal microscopy: comparisons, applications, and problems” BioTechniques 39:S2-S5 doi 10.2144/000112089

[6] J. Sharpe, U. Ahlgren, P. Perry, B. Hill, A. Ross, J. Hecksher-Sørensen, R. Baldock, and D. Davidson, (2002) “Optical projection tomography as a tool for 3D microscopy and gene expression studies,” Science 296(5567), 541–545.

[7] Wobus, A. M. and Boheler, K. R., 2005. Embryonic stem cells: prospects for developmental biology and cell therapy. Physiol Rev. 85, 635-678.

[8] Choumerianou, D. M., Dimitriou, H. and Kalmanti, M., 2008. Stem cells: promises versus limitations. Tissue Eng Part B Rev. 14, 53-60.

[9] U. J. Birk, A. Darrell, N. Konstantinides, A. Sarasa-Renedo, and J. Ripoll, (2011) “Improved reconstructions and generalized filtered back projection for optical projection tomography,” Appl. Opt. 50(4), 392–398.

[10] Severs, N. J. (2000), The cardiac muscle cell. Bioessays, 22: 188–199. doi: 10.1002/(SICI)1521-1878(200002)22:2<188::AID-BIES10>3.0.CO;2-T.

[11] D.J. Owens, J. Haning, L. Erickson-Herbrandson, and J. Aho, “Techniques for High Throughput Cardiotoxicity Studies Using Human Stem Cell-Derived Cardiomyocytes” R&D Systems, Inc., 614 McKinley PL. NE, Minneapolis, MN 55413. Available on (accessed on 17/11/15): https://www.rndsystems.com/resources/posters/techniques-high-throughput-cardiotoxicity-studies-using-human-stem-cell-derived

[12] Daniel Sinnecker, Karl-Ludwig Laugwitz, Alessandra Moretti (04.03.2014) “Induced pluripotent stem cell-derived cardiomyocytes for drug development and toxicity testing” doi:10.1016/j.pharmthera.2014.03.004

[13] Oren Caspi, Ilanit Itzhaki, Izhak Kehat, Amira Gepstein, Gil Arbel, Irit Huber, Jonathan Satin, and Lior Gepstein (January/February 2009). “Stem Cells and Development”, 18(1): 161-172. doi:10.1089/scd.2007.0280.

[14] Kehat, I., Kenyagin-Karsenti, D., Snir, M., Segev, H., Amit, M., Gepstein, A., Livne, E., Binah, O., Itskovitz-Eldor, J. and Gepstein, L., (2001). Human embryonic stem cells can differentiate into myocytes with structural and functional properties of cardiomyocytes. J Clin Invest. 108, 407-414.

[15] Mummery, C., Ward-van Oostwaard, D., Doevendans, P., Spijker, R., van den Brink, S., Hassink, R., van der Heyden, M., Opthof, T., Pera, M., de la Riviere, A. B., Passier, R. and Tertoolen, L., (2003). Differentiation of human embryonic stem cells to cardiomyocytes: role of coculture with visceral endoderm-like cells. Circulation. 107, 2733-2740.

[16] Freund, C., Davis, R. P., Gkatzis, K., Ward-van Oostwaard, D. and Mummery, C. L., (2010). The first reported generation of human induced pluripotent stem cells (iPS cells) and iPS cell-derived cardiomyocytes in the Netherlands. Neth Heart J. 18, 51-54.

[17] James E Dixon, Emily Dick, Divya Rajamohan, Kevin M Shakesheff and Chris Denning (2011) Directed Differentiation of Human Embryonic Stem Cells to Interrogate the Cardiac Gene Regulatory Network. Molecular Therapy; 19 9, 1695–1703. doi:10.1038/mt.2011.125

[18] Sakurai, T., Lanahan, A., Woolls, M. J., Li, N., Tirziu, D., Murakami, M. (2014) Live Cell Imaging of Primary Rat Neonatal Cardiomyocytes Following Adenoviral and Lentiviral Transduction Using Confocal Spinning Disk Microscopy. J. Vis. Exp. (88), e51666, doi: 10.3791/51666.

[19] Louch WE, Sheehan KA, Wolska BM (2011) Methods in cardiomyocyte isolation, culture, and gene transfer. J Mol Cell Cardiol 51: 288–298 doi: 10.1016/j.yjmcc.2011.06.01221723873

[20] Roth GM, Bader DM, Pfaltzgraff ER. (2014) Isolation and physiological analysis of mouse cardiomyocytes. J Vis Exp. 2014 Sep 7; (91):e51109. doi: 10.3791/51109.

[21] Kehat, I., Kenyagin-Karsenti, D., Snir, M., Segev, H., Amit, M., Gepstein, A., Livne, E., Binah, O., Itskovitz-Eldor, J. and Gepstein, L., 2001. Human embryonic stem cells can differentiate into myocytes with structural and functional properties of cardiomyocytes. J Clin Invest. 108, 407-414.

[22] Mummery, C., Ward-van Oostwaard, D., Doevendans, P., Spijker, R., van den Brink, S., Hassink, R., van der Heyden, M., Opthof, T., Pera, M., de la Riviere, A. B., Passier, R. and Tertoolen, L., 2003. Differentiation of human embryonic stem cells to cardiomyocytes: role of coculture with visceral endoderm-like cells. Circulation. 107, 2733-2740.

[23] Oh, H., Bradfute, S. B., Gallardo, T. D., Nakamura, T., Gaussin, V., Mishina, Y., Pocius, J., Michael, L. H., Behringer, R. R., Garry, D. J., Entman, M. L. and Schneider, M. D., 2003. Cardiac progenitor cells from adult myocardium: homing, differentiation, and fusion after infarction. Proc Natl Acad Sci U S A. 100, 12313-12318.

[24] Goumans, M. J., de Boer, T. P., Smits, A. M., van Laake, L. W., van Vliet, P., Metz, C. H., Korfage, T. H., Kats, K. P., Hochstenbach, R., Pasterkamp, G., Verhaar, M. C., van der Heyden, M. A., de Kleijn, D., Mummery, C. L., van Veen, T. A., Sluijter, J. P. and Doevendans, P. A., (2007). TGF-beta1 induces efficient differentiation of human cardiomyocyte progenitor cells into functional cardiomyocytes in vitro. Stem Cell Res. 1, 138-149.

[25] Ye, K. Y., Sullivan, K. E., Black, L. D. (2011) Encapsulation of Cardiomyocytes in a Fibrin Hydrogel for Cardiac Tissue Engineering. *J. Vis. Exp.* (55), e3251, doi: 10.3791/3251.

[26] Smith, A. M., R. M. Shelton, et al. (2007). "An initial evaluation of gellan gum as a material for tissue engineering applications." J Biomater Appl 22(3): 241-254.

[27] Silva, N. A., A. J. Salgado, et al. (2010). "Development and characterization of a novel hybrid tissue engineering-based scaffold for spinal cord injury repair." Tissue Eng Part A 16(1): 45-54

[28] Harrison, R.G. et al. (1907) “Observations of the living developing nerve fiber.” Anat. Rec. 1, 116–128

[29] Harrison, R.G. (1910) “The outgrowth of the nerve fiber as a mode of protoplasmic movement.” J. Exp. Zool. 9, 787–846

[30] Susan Breslin and Lorraine O’Driscoll (March, 2013), “Three dimensional cell culture: the missing link in drug discovery” Drug Discovery Today – 18 (5-6): 241-249.

[31] Mei Jeng-Chun, Wu Aden Yuan Kun, Wu Po-Chen, Cheng Nai-Chen, Tsai Wei-Bor, and Yu Jiashing. (November 2014), “Three-Dimensional Extracellular Matrix Scaffolds by Microfluidic Fabrication for Long-Term Spontaneously Contracted Cardiomyocyte Culture” Tissue Engineering Part A 20(21-22): 2931-2941. doi:10.1089/ten.tea.2013.0549.

[32] Weaver, V.M. et al. (1997) “Reversion of the malignant phenotype of human breast cells in three-dimensional culture and in vivo by integrin blocking antibodies.” J. Cell Biol. 137, 231–245

[33] Robert E. Akins, Jr., Danielle Rockwood, Karyn G. Robinson, Daniel Sandusky, John Rabolt, and Christian Pizarro. (February 2010) “Tissue Engineering Part A”. 16(2): 629-641. doi:10.1089/ten.tea.2009.0458

[34] Messner S., Agarkova I., Moritz W., Kelm J. M. (2013) “Multi-cell type human liver microtissues for hepatotoxicity testing.” Arch. Toxicol. 87, 209–213

[35] Shaked NT, Satterwhite LL, Bursac N, Wax A. (2010) Whole-cell-analysis of live cardiomyocytes using wide-field interferometric phase microscopy. Biomedical Optics Express; 1(2):706-719. doi:10.1364/BOE.1.000706.

[36] Marquet P., Rappaz B., Magistretti P. J., Cuche E., Emery Y., Colomb T., Depeursinge C. (2005), “Digital holographic microscopy: a noninvasive contrast imaging technique allowing quantitative visualization of living cells with subwavelength axial accuracy,” Opt. Lett. 30(5), 468–470 10.1364/OL.30.000468

[37] Shaked, N. T., Finan, J. D., Guilak, F., & Wax, A. (2010). Quantitative phase microscopy of articular chondrocyte dynamics by wide-field digital interferometry. *Journal of Biomedical Optics*, *15*(1), 010505. http://doi.org/10.1117/1.3290242

[38] Popescu G., Park Y., Lue N., Best-Popescu C., Deflores L., Dasari R. R., Feld M. S., and Badizadegan K., (2008) “Optical imaging of cell mass and

growth dynamics," Am. J. Physiol.: Cell Physiol.295(2), C538–C544.10.1152/ajpcell.00121.2008

[39] Tomohiro Hayakawaa, Takeshi Kunihiroa , Tomoko Andob, Seiji Kobayashia, Eriko Matsuia, Hiroaki Yadaa, Yasunari Kandab, Junko Kurokawab, Tetsushi Furukawab (2014), "Image-based evaluation of contraction–relaxation kinetics of human-induced pluripotent stem cell-derived cardiomyocytes: Correlation and complementarity with extracellular electrophysiology" doi:10.1016/j.yjmcc.2014.09.010

[40] Tomohiro Hayakawaa, Takeshi Kunihiroa , Suguru Dowaki, Hatsume Uno, Eriko Matsui, Masashi Uchida (2011) "Noninvasive Evaluation of Contractile Behavior of Cardiomyocyte Monolayers Based on Motion Vector Analysis" Life Science Laboratory, Advanced Material Laboratories, Sony Corporation, Tokyo, Japan. Tissue Engineering Part C Methods (Impact Factor: 4.64). 08/2011; 18(1):21-32. DOI: 10.1089/ten.TEC.2011.0273

[41] Wright, S. J., V. E. Centonze, S. A. Stricker, P. J, DeVries, S. W. Paddock, and G. Schatten. 1993. An introduction to confocal microscopy and three-dimensional reconstruction. Methods Cell Bio. 38:1-45.

[42] Azeloglu E. U., Costa K. D. (2010), "Cross-bridge cycling gives rise to spatiotemporal heterogeneity of dynamic subcellular mechanics in cardiac myocytes probed with atomic force microscopy," Am. J. Physiol. Heart Circ. Physiol. 298(3), H853–H860.10.1152/ajpheart.00427.2009

[43] Rajala, K., Pekkanen-Mattila, M., & Aalto-Setälä, K. (2011). Cardiac Differentiation of Pluripotent Stem Cells. Stem Cells International, 2011, 383709. doi:10.4061/2011/383709

[44] Passier, R., Oostwaard, D. W., Snapper, J., Kloots, J., Hassink, R. J., Kuijk, E., Roelen, B., de la Riviere, A. B. and Mummery, C., (2005). Increased cardiomyocyte differentiation from human embryonic stem cells in serum-free cultures. Stem Cells. 23, 772-780.

[45] Graichen, R., Xu, X., Braam, S. R., Balakrishnan, T., Norfiza, S., Sieh, S., Soo, S. Y., Tham, S. C., Mummery, C., Colman, A., Zweigerdt, R. and Davidson, B. P., 2008. Enhanced cardiomyogenesis of human embryonic stem cells by a small molecular inhibitor of p38 MAPK. Differentiation. 76, 357-370.

[46] Mummery, C., Ward-van Oostwaard, D., Doevendans, P., Spijker, R., van den Brink, S., Hassink, R., van der Heyden, M., Opthof, T., Pera, M., de la Riviere, A. B., Passier, R. and Tertoolen, L., (2003). Differentiation of human

embryonic stem cells to cardiomyocytes: role of coculture with visceral endoderm-like cells. Circulation. 107, 2733-2740.

[47] Xu, X. Q., Graichen, R., Soo, S. Y., Balakrishnan, T., Rahmat, S. N., Sieh, S., Tham, S. C., Freund, C., Moore, J., Mummery, C., Colman, A., Zweigerdt, R. and Davidson, B. P., (2008). Chemically defined medium supporting cardiomyocyte differentiation of human embryonic stem cells. Differentiation. 76, 958-970.

[48] Edite Figueiras, Ana M. Soto, Danilo Jesus, M. Lehti, J. Koivisto, J.E Parraga, J. Silva-Correia, J.M. Oliveira, R. L. Reis, M. Kellomäki, and J. Hyttinen , (1 October 2014) "Optical Projection Tomography as a tool for 3D imaging of hydrogels." | Vol. 5, No. 10 | DOI:10.1364/BOE.5.003443 | BIOMEDICAL OPTICS EXPRESS 3443

[49] PIV (Particle Image Velocimetry) --- ImageJ plugin. Available on (accessed on 03/11/15): https://sites.google.com/site/qingzongtseng/piv

[50] J. Soria (1996) "An investigation of the near wake of a circular cylinder using a video-based digital cross-correlation particle image velocimetry technique" Exp. Thermal Fluid Sci., 12 (2), pp. 221–233

[51] Q. Tseng, E. Duchemin-Pelletier, A. Deshiere, M. Balland, H. Guillou, O. Filhol, et al. (Jan 31 2012), "Spatial organization of the extracellular matrix regulates cell–cell junction positioning" Proc Natl Acad Sci U S A, 109 (5) pp. 1506–1511

[52] Traction Force Microscopy. Available on (accessed on 03/11/15): https://sites.google.com/site/qingzongtseng/tfm

[53] B. Sabass, M. L. Gardel, C. Waterman and U. S. Schwarz (2008) "High resolution traction force microscopy based on experimental and computational advances." Biophys. J., 94:207-220.

[54] Ahearne, M., Yang, Y., El Haj, A. J., Then, K. Y., & Liu, K.-K. (2005). Characterizing the viscoelastic properties of thin hydrogel-based constructs for tissue engineering applications. *Journal of the Royal Society Interface*, *2*(5), 455–463. http://doi.org/10.1098/rsif.2005.0065

[55] Indradumna Banerjee, (03/09/2014) "Measurement of beating force of cardiomyocytes using an atomic force microscope". Available on (accessed on 17/11/15): http://URN.fi/URN:NBN:fi:tty-201408271405

APPENDIX A: PREPARATION OF STOCK SOLUTIONS FOR GELLAN GUM HYDROGELS

Preparation of stock solutions

The stock solutions made for the preparation of hydrogels are made in 10 % sucrose aqueous solution, sterile filtered and then stored in a refrigerator at +4 degree centigrade. Hence, the very first step is to make a 10 % sucrose aqueous solution, followed by making the stock solutions of gellan gum and spermine.

10 % Sucrose aqueous solution

Sucrose is weighed in a powdered form with 1g/10mL of the wanted solution. Hence, we weighed 10g of sucrose to make 100mL of sucrose aqueous solution. After weighing, it is poured in a volumetric flask and distilled water (100mL) is added to the flask. To make sure the sucrose gets completely dissolved in the water, the flask is shaken and turned upside down until the sucrose gets dissolved fully. After the dissolving of the sucrose, the sucrose solution is sterile filtered.

Gellan gum stock solution

Gellan gum is weighed with 5mg/mL of the wanted solution. Hence, we weighed 250mg of gellan gum to make 50mL of stock solution. After weighing the powdered gellan gum, it is poured in the decanter glass and then 50 mL of 10% sucrose solution is added to the glass to make 50mL of gellan gum solution with 250mg/50mL concentration. Since, it is not easy to dissolve gellan gum by mere shaking or mixing, the magnetic stirrer is added to the glass and glass is covered with the parafilm. Afterwards, the glass is kept at magnetic stirrer overnight so the next day, the gellan gum stock solution is completely ready with gellan gum completely dissolved in a 10% sucrose solution. The stock solution is then sterile filtered by first heating the gellan gum solution at 60 degree centigrade, in a water bath.

Spermine stock solution

Spermine in a powdered form is weighed with 1.4mg/mL of the wanted concentration. Hence, we weighed 14mg of spermine to make 10ml of spermine stock solution. After weighing, spermine is put in a volumetric flask and 10% sucrose solution (10mL in our case) is added to it. Unlike gellan gum, Spermine is easily dissolved and then, sterile filtered and stored at +4 degree centigrade. In addition, spermine is further diluted in 10% sucrose into final concentration which is normally 0.35mg/mL. The diluted spermine is also stored in the refrigerator at +4 degree centigrade.

Gellan gum, sucrose and spermine are obtained in a powdered form from the manufacturer Sigma Aldrich. In addition, stock solutions for spermine and sucrose are prepared and mixed immediately while gellan gum stock solution is kept on a magnetic stirrer for overnight stirring. These stock solutions, once ready, are used to prepare hydrogels as described in chapter 3. Figure 18 briefly illustrates the process of preparation of gellan gum stock solutions.

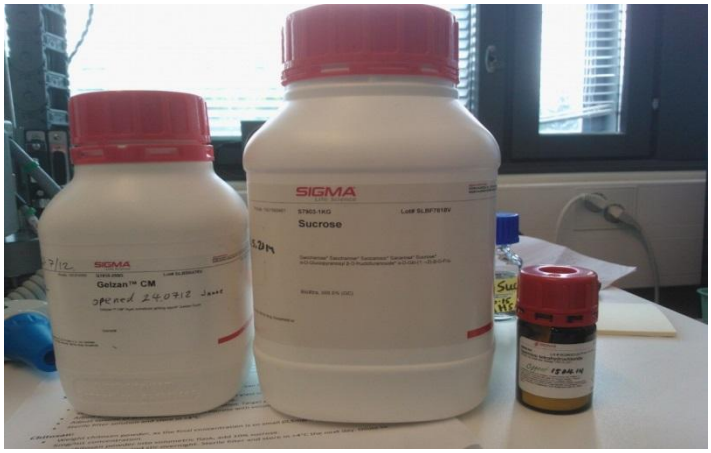

a) From Left to Right; Gellan gum, Sucrose and Spermine in a powdered form

b) Gellan gum stock solution kept at magnetic stirrer for overnight stirring

Figure 18. *The overview of stock solution preparation, in picture*

APPENDIX B: 3D CONSTRUCTS OF THE SAMPLES USING IMAGEJ

For instance, we decided to retrieve the 3D volume plots in a video format of one sample for all 600 frames. At first we took the 3D plot of the gel area at 1/600th frame when the cells were not beating and the gel was having no impact from the cells. This 3D plot at 1/600th frame is being shown in Figure 19.

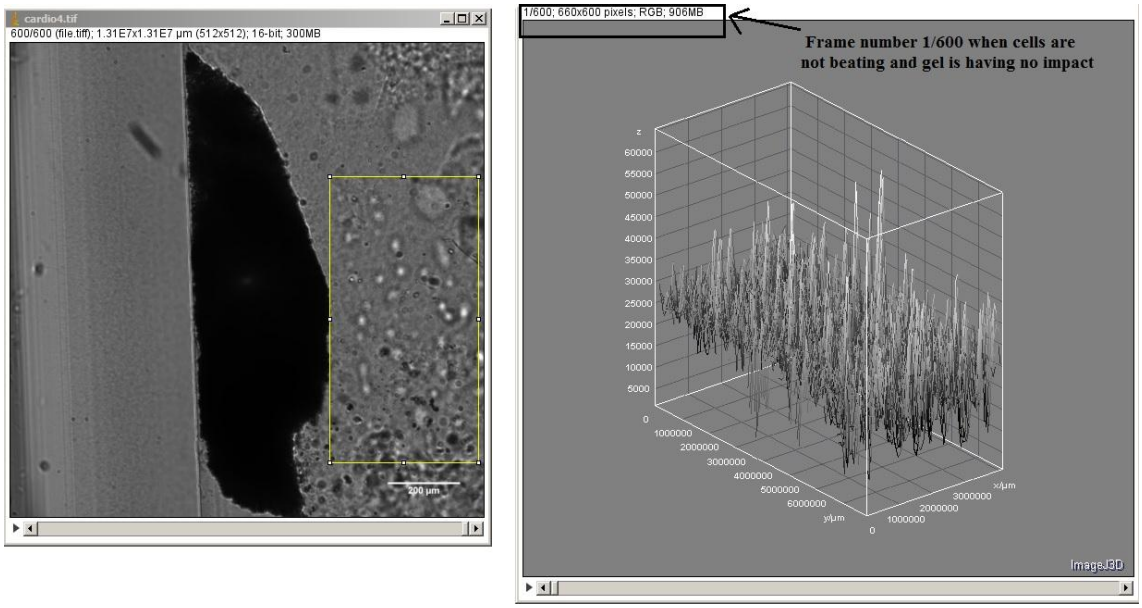

Figure 19. *Qualitative 3D plot illustration of the gel around the beating cluster, when the cells are relaxed and having no impact of beating*

After taking this still image at 1/600th frame, we went on with the 3D video plot and at 199/600th frame, when the cells encountered beating, we noticed a visible change in the 3D plot of the gel area around the cells. This is being shown in Figure 20.

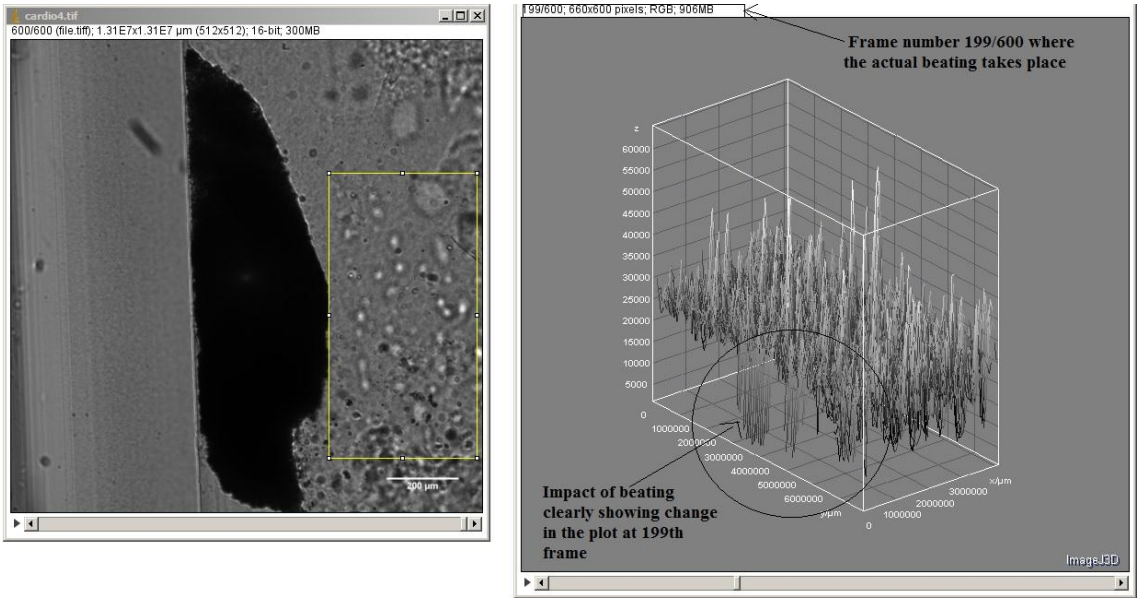

Figure 20. *3D plot of the gel at 199/600th frame, illustrating an impact of beating cells*

This impact and change in the 3D volume plot of the gel area as shown by rectangular portion around the cell can be illustrated better with the illustration of both the 3D volume plots side-by-side. This is illustrated in Figure 21.

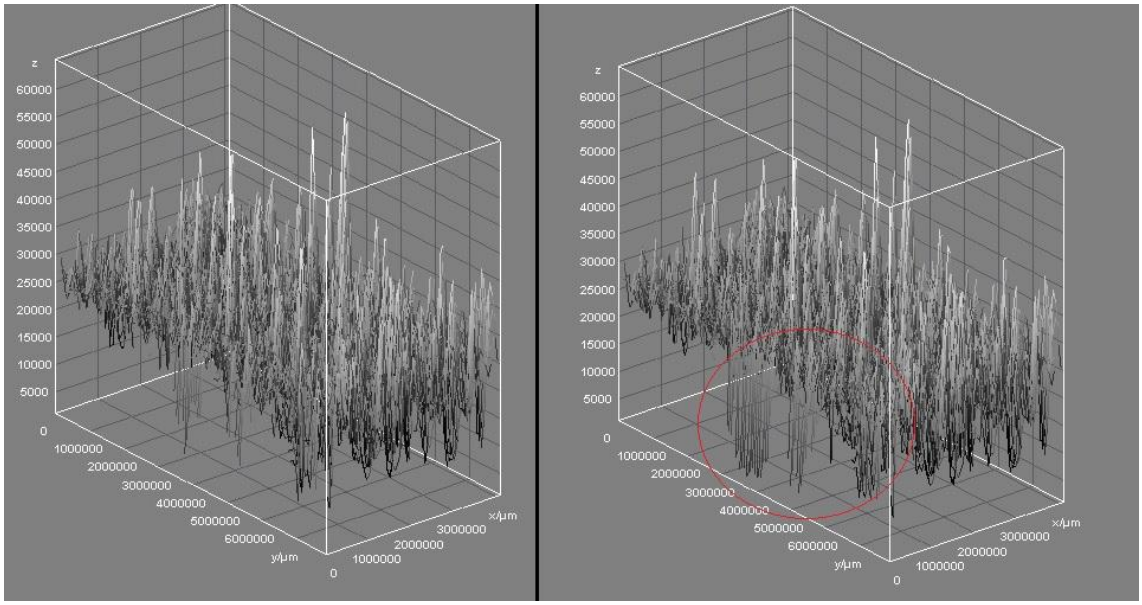

Figure 21. *3D volume plot of gel area without beating (Left) versus 3D volume plot of gel area with an impact of beating (Right)*

The circular portion in Figure 21 shows the change in the volume plot of the cell. It must also be noted that the portion of the gel which was right around the beating clus-

ters exhibited the change in their volume plot while the rest of the area of the gel shows more or less the same plot in both the cases.

In addition, the beating pattern of the cardiomyocytes affects the gel as the gel experiences the traction force, due to which the area surrounding the impact will show a slightly different pattern, as shown in Figure 22.

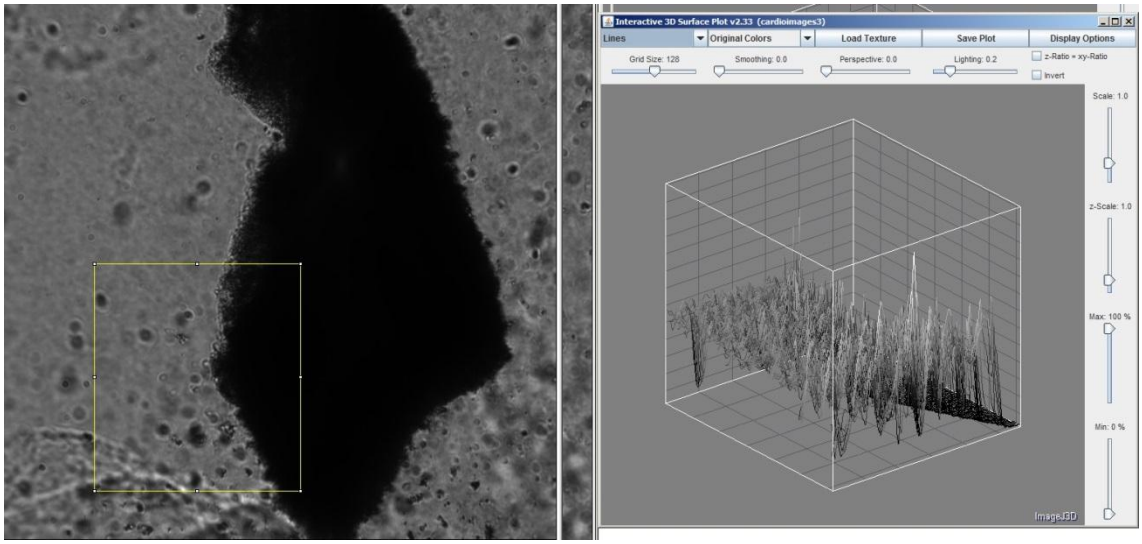

Figure 22. *A 3D construct of the specific area of the gel surrounding the beating cluster*

In Figure 22, the area that was having an impact of the beating cluster was selected for the analysis, as shown from the rectangle. A 3D construct of the chosen area was created. The black dark shade on the bottom shows the area of the cluster of beating cells that was having an impact on the surrounding gel due to the traction force of the cardiomyocytes. When the beating of the cardiomyocytes takes place, the surrounding gel experiences a traction force and the gel itself represents a contraction and relaxation phase.

The qualitative difference in the pattern can be seen properly in Figure 23.

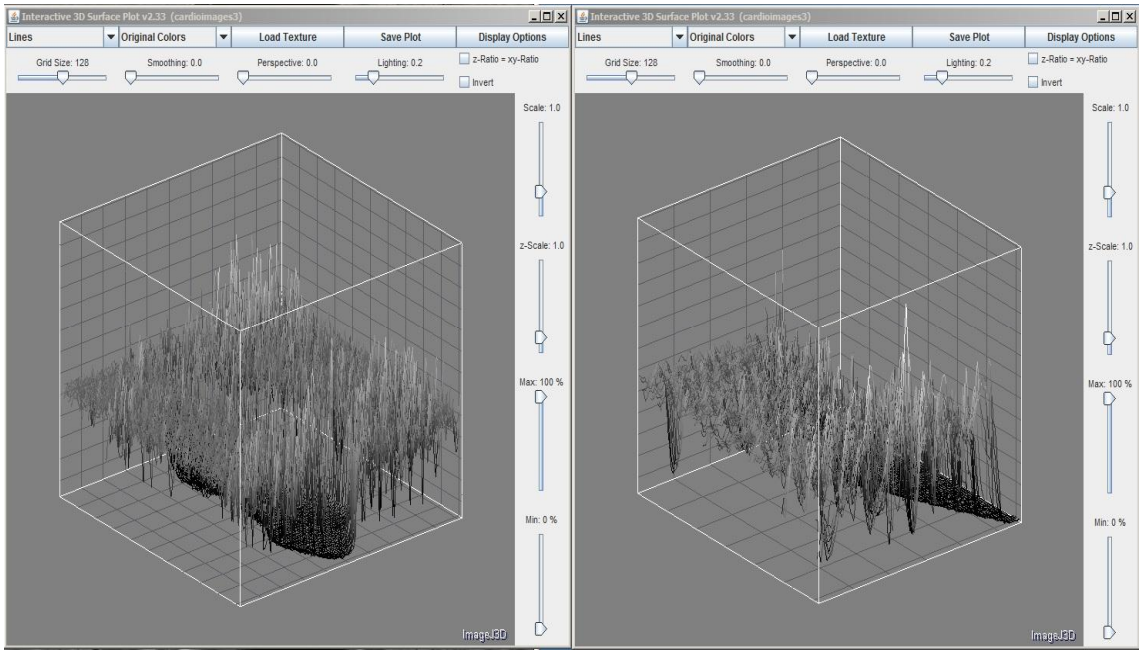

Figure 23. *Comparison of 3D constructs of a gel on the whole (left) and gel area surrounding the beating cells (right)*

APPENDIX C: MORE RESULTS AND CALCULATIONS

Some other acquisitions that we obtained are being shown in Figure 24.

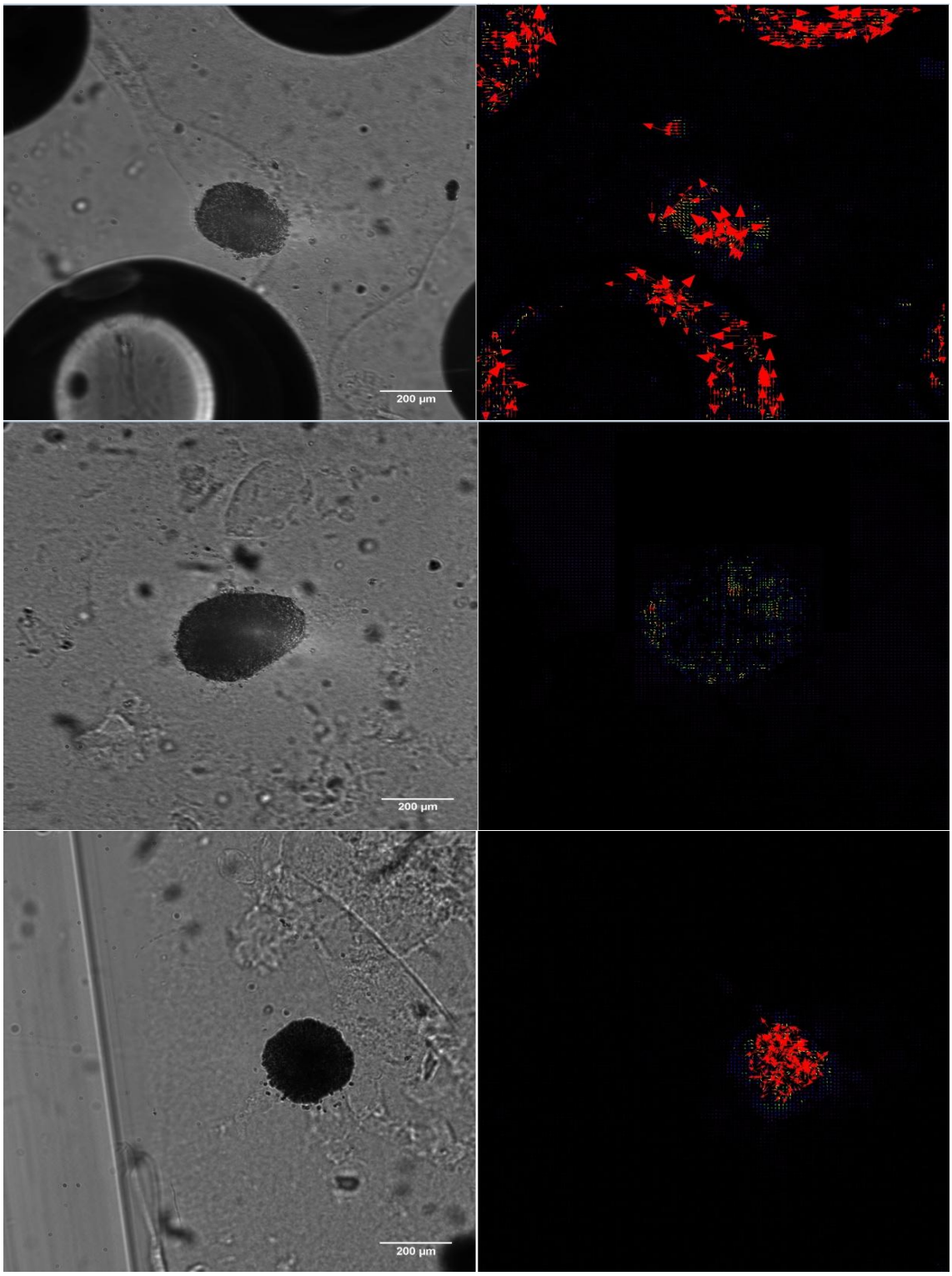

Figure 24. *More acquisitions with vector-representation*

In Figure 24, it can also be seen that one sample containing air bubbles is also showing velocity vectors for the air bubbles since they were also moving inside the sample.

First medium sized sample at 180 degree (Average traction force calculation)

Data Set:
92.81748962402344, 194.69290161132812, 122.7305679321289, 40.93564224243164, 109.07845306396484, 232.78907775878906, 63.61727523803711, 113.97127532958984, 38.32958984375, 61.56666564941406, 178.52276611328125, 279.1968994140625, 352.6536865234375, 126.87106323242188, 74.53694915771484, 58.78879928588867, 82.14646911621094, 184.4287872314453, 156.31976318359375, 139.96258544921875

Average (Mean):

Count: **20**

Sum: **2703.9567070007**

Average: **2703.9567070007 / 20 = 135.19783535004**

135.19 Pascal = 0.14 mN/ mm²

First medium sized sample at 270 degree (Average traction force calculation)

Data Set:
163.0885467529297, 1045.10009765625, 1620.6727294921875, 2853.323486328125, 1411.66357421875, 2330.315185546875, 2429.7373046875, 1207.570556640625, 744.4255981445312, 375.0946960449219, 1649.603271484375, 204.8759002685547, 149.54598999023438, 262.3087463378906, 36.8996696472168, 57.20319366455078, 339.6070556640625, 1147.72509765625, 1548.255615234375, 1154.5047607421875

Average (Mean):

Count: **20**

Sum: **20731.521076202**

Average: **20731.521076202 / 20 = 1036.5760538101**

1036.57 Pascal = 1.03 mN/ mm²

First medium sized sample at 280 degree (Average traction force calculation)

Data Set:
132.60104370117188, 78.39693450927734, 221.75949096679688, 89.37909698486328, 65.09110260009766, 506.19940185546875, 213.8173828125, 55.63587951660156, 117.84228515625, 510.732421875, 219.92434692382812, 526.4728393554688, 372.3918151855469, 154.51023864746094, 301.1058654785156, 429.077880859375, 227.70303344726562, 532.8986206054688, 731.6104736328125, 828.176025390625

Average (Mean):

Count: **20**

Sum: **6315.3261795044**

Average: **6315.3261795044 / 20 = 315.76630897522**

315.76 Pascal = 0.31 mN/ mm²

Second medium sized sample (Average traction force calculation)

Data Set:
120.39239501953125, 41.62598419189453, 197.42361450195312, 240.12680053710938, 120.00456237792969, 397.03192138671875, 229.89268493652344, 310.0093994140625, 297.1102294921875, 231.7427520751953, 153.79530334472656, 56.96299743652344, 269.1953125, 74.80231475830078, 125.88256072998047, 153.71595764160156, 121.55502319335938, 27.622196197509766, 18.323604583740234, 6.725365161895752

Average (Mean):

Count: **20**

Sum: **3193.9409794807**

Average: **3193.9409794807 / 20 = 159.69**

159.69 Pascal = 0.2 mN/ mm²

Second small sized sample (Average traction force calculation)

Data Set:
116.05254364013672, 79.53546905517578, 190.85325622558594, 73.27948760986328, 144.55581665039062, 82.5748291015625, 56.021060943603516, 147.5044403076172, 151.2896728515625, 124.54727935791016, 131.28887939453125, 31.836074829101562, 16.067962646484375,

33.31089782714844, 45.22353744506836, 26.04768943786621, 28.895130157470703, 19.335187911987305, 18.162107467651367, 15.780129432678223

Average (Mean):

Count: **20**

Sum: **1532.1614522934**

Average: **1532.1614522934 / 20 = 76.60807261467**

76.60 Pascal = 0.07 mN/ mm²

Temperature based average traction force calculation (at 37 degree centigrade)

Data Set:
714.0186157226562, 696.09521484375, 1150.6524658203125, 683.6880493164062, 498.3047180175781, 741.710693359375, 1096.210205078125, 1032.1141357421875, 861.0938720703125, 757.7919921875, 386.36041259765625, 515.406982421875, 216.0012969970703, 75.62415313720703, 38.46397399902344, 348.0347595214844, 862.4340209960938, 207.04153442382812, 140.23187255859375, 220.87709045410156

Average (Mean):

Count: **20**

Sum: **11242.156059265**

Average: **11242.156059265 / 20 = 562.10**

562.10 Pascal = 0.56 mN/ mm²

Temperature based average traction force calculation (at 32 degree centigrade)

Data Set:
436.55352783203125, 144.96493530273438, 575.9484252929688, 924.857177734375, 1071.051025390625, 446.3847961425781, 385.9530029296875, 217.26332092285156, 220.3404083251953, 733.2598876953125, 990.077880859375, 278.547119140625, 457.7724304199219, 769.2505493164062, 630.649658203125, 599.7376098632812, 365.400146484375, 360.67059326171875, 332.0064697265625, 1071.746826171875

Average (Mean):

Count: **20**

Sum: **11012.435791016**

Average: **11012.435791016 / 20 = 550.62**

550.62 Pascal = 0.55 mN/ mm²

Temperature based average traction force calculation (at 27 degree centi-grade)

Data Set:
1077.8486328125, 1109.631103515625, 994.40576171875, 546.9768676757812, 675.5263671875, 101.28892517089844, 114.37445068359375, 334.2792053222656, 311.4933776855469, 347.07208251953125, 220.73077392578125, 313.5124816894531, 90.93601989746094, 278.90118408203125, 229.97509765625, 341.1365661621094, 197.81024169921875, 115.15277862548828, 207.5428924560547, 787.0261840820312

Average (Mean):

Count: **20**

Sum: **8395.6209945679**

Average: **8395.6209945679 / 20 = 419.78 Pascal**

419.78 Pascal = 0.42 mN/ mm²